

Modelling of Whiplash Trauma

Parametric study of rear-end impacts using FEM and CFD

Master's Thesis in the Automotive Engineering Master Programme

Andreu Oliver González

Mourya Vanama

Department of Applied Mechanics

Division of Fluid Dynamics/Division of Vehicle Safety

CHALMERS UNIVERSITY OF TECHNOLOGY

Göteborg, Sweden 2010

Master's Thesis 2010:22

Master's Thesis 2010:22

Modelling of Whiplash Trauma

Parametric study of rear-end impacts using FEM and CFD

Master's Thesis in the Automotive Engineering Master Programme

Andreu Oliver González

Mourya Vanama



Department of Applied Mechanics
Division of Fluid Dynamics/Division of Vehicle Safety
Chalmers University of Technology
Göteborg, Sweden 2010

Modelling of Whiplash Trauma

Parametric study of rear-end impacts using FEM and CFD

Master's Thesis in the Automotive Engineering Master Programme

Andreu Oliver González

Mourya Vanama

© Andreu Oliver González, Mourya Vanama, 2010

Master's Thesis 2010:22

ISSN 1652-8557

Department of Applied Mechanics

Division of Fluid Dynamics/Division of Vehicle Safety

Chalmers University of Technology

SE-412 96 Göteborg

Sweden

Telephone: + 46 (0)31-772 1000

Cover:

FE simulation of THUMS model in rear-end impact for an acceleration pulse of 5g (above) and simulation of the blood vessels network surrounding the spinal canal for acceleration pulse of 5g (below).

Chalmers Reproservice

Göteborg, Sweden 2010

Modelling of Whiplash Trauma

Parametric study of rear-end impacts using FEM and CFD

Master's Thesis in the Automotive Engineering Master Programme

Andreu Oliver González

Mourya Vanama

Department of Applied Mechanics

Division of Fluid Dynamics/Division of Vehicle Safety

Chalmers University of Technology

Abstract

This work is a combination of Finite Element (FE) modelling and Computational Fluid Dynamics (CFD) to investigate the effect of acceleration pulses, head restraint and seating posture on facet joint loads and pressure transient magnitudes on the neck injury outcome during whiplash motion.

A parametric study is carried out with the FE human body model THUMS (Total HUMAN Model for Safety) for a variety of crash pulses and crash conditions that have a known relative risk of long term neck injuries in rear-end impacts. The injury criterion NIC (Neck Injury Criteria) is addressed for the studies made.

The THUMS model is used to generate the motion data of the spinal canal, which is used as an input to simulate the behaviour of the spinal canal to analyse the pressure transients in the network of blood vessels during the whiplash motion performing CFD simulations using the OpenFOAM CFD toolbox. Using the output of FE simulations, a moving mesh technique is used to achieve the motion of the mesh points in the CFD simulations.

The results give an insight into proposed injury mechanisms and injury risk assessment criteria concerning long term neck injuries. The effect of head restraint and its position with respect to the driver's head in mitigating the above injuries is discussed for different crash scenarios.

Key words: Neck Injuries, Whiplash Trauma, FEM, CFD, THUMS, NIC, Facet Joint Strains and Injury Mechanism

Contents

Abstract	I
Preface	V
Acknowledgements	VII
Nomenclature	IX
1 Introduction	1
1.1 Background	1
1.2 Anatomy of the Human Vertebral Column	2
1.3 Rear-end Impacts	4
1.3.1 Occupant Kinematics	4
1.3.2 Injury Mechanisms	5
1.3.3 Injury Severity	5
1.4 Neck Injury Criterion and Tolerance Levels	6
1.5 Facet Joint Capsule Strain	7
1.6 Objective	8
2 Methodology	9
2.1 FE Modelling	9
2.1.1 THUMS	9
2.1.2 Driver Seat	10
2.2 Crash Pulses	10
2.3 Parametric Study	11
2.4 CFD Modelling of the Venous Plexus	12
2.4.1 Theoretical Model	12
2.4.2 Geometrical Modelling	13
2.4.3 Kinematic Modelling	18
2.4.4 Definition of the Fluid Dynamic Properties	21
2.4.5 Solver and Numerical Schemes	22
3 Results and Discussions	24
3.1 Motion	24
3.2 FE simulations	27
3.2.1 Neck Injury Criterion (NIC)	27
3.2.2 Influence of Head Restraint Position and Occupant Posture	29
3.2.3 Facet Joint Strains	31
3.3 CFD simulations	35
3.3.1 Convergence	35
3.3.2 Behaviour of the Pressure	35
3.3.3 Behaviour of the Velocity	37

4	Conclusion	40
5	Future Scope	41
6	References	42
6.1	Publications	42
6.2	Internet References	46
	Appendix A	i
	Facet Joint Capsule Strains for 2.5 and 7.5g with and without Head Restraint	i
	Appendix B	vii
	Blood Flow Through the Model	vii

Preface

The current work is a study on the whiplash motion taking place in rear-end impacts to investigate the effect of different parameters on facet joint loads and pressure transient magnitudes. The research commenced in January 2010 and presented on 7th of June 2010. The study is a part of ADSEAT research project, which is a European Commission funded project. ADSEAT project aims to improve seat design for reducing whiplash injury. The project is carried out at the Departments of Fluid Dynamics and Vehicle and Traffic Safety Centre (SAFER) of Chalmers University of Technology (Göteborg, Sweden).

The work has been supervised by Professor Lars Davidson, Professor Mats Svensson, Associate Professor Håkan Nilsson, Adjunct Professor Lotta Jakobsson and Ph.D. student Kristian Holmqvist.

Göteborg June 2010

Andreu Oliver González / Mourya Vanama



Acknowledgements

This work is a cross-divisional project between the divisions of Fluid Dynamics and the division of Vehicle Safety at Chalmers University of Technology (Göteborg, Sweden). We are very grateful to all the people that have followed and helped us on our way in this project.

We are very thankful to our supervisors: Professor Lars Davidson, Professor Mats Svensson and Associate Professor Håkan Nilsson who were instrumental in providing us with an opportunity to work for this cross-divisional project. We also express our gratitude to them for providing us with invaluable knowledge and guidance throughout this project. In addition, we are grateful to Assistant Professor Johan Davidsson, Assistant Professor Karin Brolin and Adjunct Professor Lotta Jakobsson for their support and guidance in this project.

We owe a special gratitude to Associate Professor Håkan Nilsson and Ph.D. student Kristian Holmqvist for their everlasting support throughout the project without which we would not have been able to complete the project on schedule.

We also thank Chalmers Center for Computational Science and Engineering (C³SE) and Swedish National Infrastructure for Computing (SNIC) for providing us with computational resources.

We are grateful to the department of Applied Mechanics for funding this project.

Our appreciation for the cooperation to our colleagues and staff in the respective offices (Johanneberg campus and SAFER) that have contributed to a very pleasant atmosphere at our working place.

We are indebted to our parents and siblings for their continuous encouragement and moral support during our education and thesis.

We express our pleasure in thanking our friends: Dr. V. V Rao, Vasantha, Gautam, Vineeth, Akshay, Xavier, Jano, Gerard, Elena, Irene, Sergio, Maria, Jessica and Lefteris, Henrik and Alexey for their company and support during our stay in Sweden.

Nomenclature

d	Distance
delta-V	Change in velocity
F	Force
g	Acceleration of gravity (9.81 m/s ²)
h	Characteristic dimension
M	Moment
R	Rotational matrix
r	Radius
Re	Reynolds number
X	X coordinate
Y	Y coordinate
Z	Z coordinate
U	Velocity
γ	Rotation around Z
θ	Rotation around Y
ϕ	Diameter
φ	Rotation around X
μ	Dynamic viscosity
ν	Kinematic viscosity
ρ	Density
$\partial/\partial t$	Partial derivative with respect to time
$\partial/\partial x$	Partial derivative with respect to space

Abbreviations

AIS	Abbreviated Injury Scale
AIS 1	Neck strain without fracture or dislocation neck injury (WAD)
C1 – C7	Cervical Vertebrae
CAD	Computational Aided Design
CFC	Channel Frequency Class (digital filter)
CFD	Computational Fluid Dynamics
CSF	Cerebral Spinal Fluid
FE	Finite Element
N_{km}	Injury criterion for assessing whiplash severity
NHTSA	National Highway Traffic Safety Administration
NIC	Neck Injury Criterion
PISO	Pressure-Implicit Split-Operator
SIMPLE	Semi-Implicit Method for Pressure-Linked Equations
T1	First Thoracic Vertebra (the top one)
THUMS	Total HUMAN Model for Safety
WAD	Whiplash Associated Disorder

1 Introduction

This section introduces to the basic knowledge of the whiplash injuries and their mechanisms.

1.1 Background

Whiplash injuries, also known as Whiplash Associated Disorders (WAD), are the most frequently reported injuries in traffic accidents involving low speed rear-end impacts. More than one million European citizens suffer from whiplash injuries each year (Capon *et al.*, 2001). In Europe, a high cost up to 10 billion euros per year is expected due to WAD. According to the research by National Highway Traffic Safety Administration (NHTSA, 1996), these injuries result in very high socio and economic costs of around \$4.5 billion per year in USA.

Generally WADs result in short term injuries. However, according to some research publications such as a study by Whiplash Kommissionen (2006) a number of cases involving lifelong consequences due to whiplash injuries are observed. A study by Krafft *et al.* (2004) reveals that in modern Swedish car market, whiplash injuries account for approximately 70% of all injuries that lead to disability.

Approximately 65% of the injuries that occur due to traffic accidents are whiplash injuries (EASI, 2007). Approximately 80% of all injuries occurring in rear-end collisions are whiplash injuries (EASI, 2007). Women tend to have a higher risk of WAD compared to men (Hell *et al.*, 1999, Jakobsson *et al.*, 2000 and Krafft *et al.*, 2004).

1.2 Anatomy of the Human Vertebral Column

The human spine is made up of 24 spinal bones, called vertebrae, which are joined together to form the spinal column, see Figure 1. The spinal column is divided into cervical spine (C1 to C7), thoracic spine (T1 to T12) and lumbar spine (L1 to L5).

The first seven vertebrae C1 to C7 form the cervical spine, shown in Figure 1. The cervical spine starts from a point where the uppermost vertebra (C1) connects to the bottom of the skull. The cervical spine ends at the conjunction of C7 to the top of the thoracic spine, called T1 vertebra.

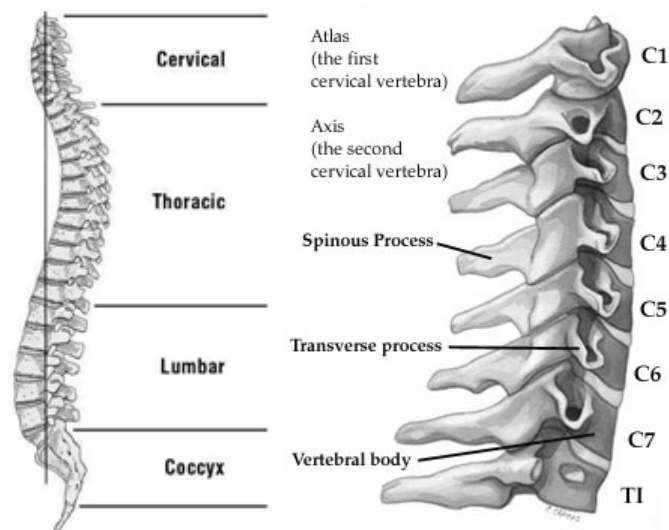


Figure 1 Human spinal column (left), Cervical Spine (right) (Hughston Health Alert)

When the vertebrae are stacked on top of each other, the bony rings form a hollow tube. This hollow tube houses the spinal cord. These vertebrae protect the spinal cord.

The spinal cord consists of millions of nerve fibres which transmit electrical pulses to the limbs, trunk and the organs of the body from the brain and vice versa. It extends from the brain down to the middle of the back, the level of the first or second lumbar vertebra just inferior of the ribs. The spinal cord, like the brain, is covered by three connective-tissue envelopes called the meninges (pia mater, arachnoid and dura mater), see Figure 2. The dura mater is the most external layer and the space between this and the surrounding bone of the vertebrae is called epidural space, where adipose tissue and a network of blood vessels are found. In between this outer envelope and the middle one, called subarachnoid space, there is the Cerebral Spinal Fluid (CSF), a clear and colourless fluid whose function is to damp and protect the nerve tissues against the damage from contacting the vertebrae.

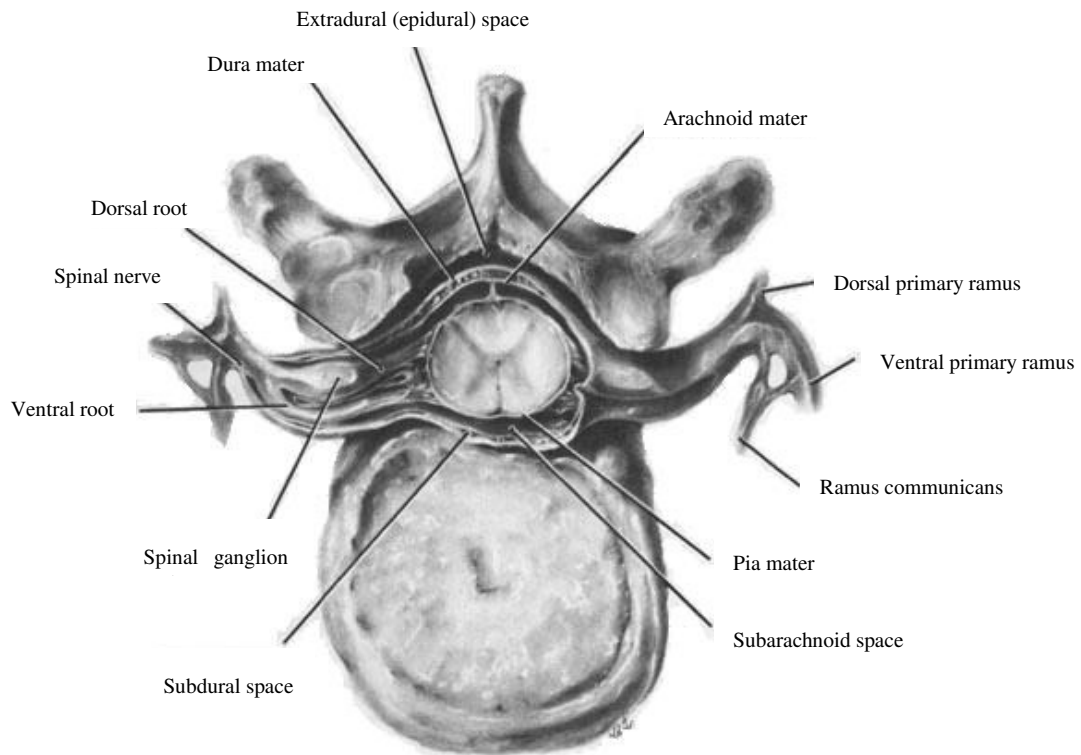


Figure 2 A horizontal cross-section of a vertebra with the soft tissues of the spinal canal (Image-Guided Musculoskeletal Procedures)

As spinal cord stretches from the brain down through the spine, it sends out nerve branches between each vertebra called nerve roots. Those arising out of the cervical spine form the nerves that go to the arms and various organs of the body as shown in Figure 3. The spinal nerves exit on laterally on either sides of the spinal segment.

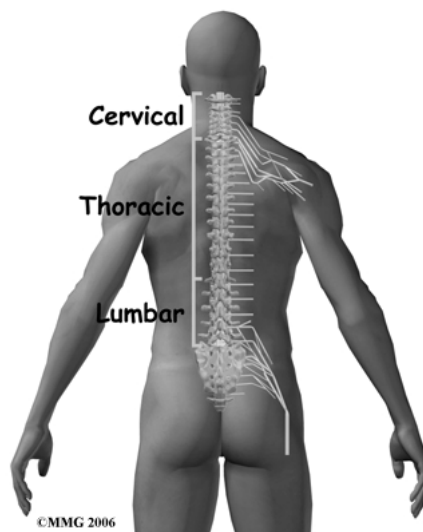


Figure 3 Nerves from spinal cord to arms (UHN Orthopaedics)

Each vertebra is separated by an intervertebral disc. There are two facet joints between each pair of vertebrae one on either sides of the spine as shown in Figure 4. The surfaces of the facet joints are covered by articular cartilage, which is a smooth,

rubbery material that covers the ends of most joints. It allows the bone ends to move against each other smoothly, without pain. The alignment of the facet joints of the cervical spine allows freedom of movement as you bend and turn your neck.

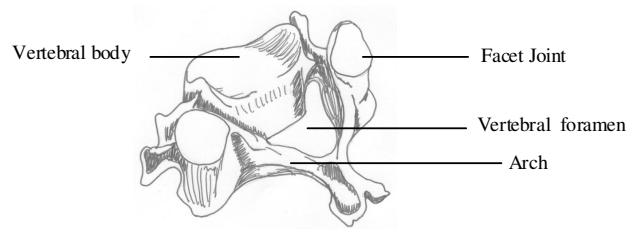


Figure 4 Location of facet joint

1.3 Rear-end Impacts

This section describes the occupant kinematics in a rear-end impact and related injuries.

1.3.1 Occupant Kinematics

Extensive research on occupant motion in rear-end impacts has been performed by several researchers (Siegmund *et al.*, 1997, Brault *et al.*, 1998, Yoganandan *et al.*, 1998, Hell *et al.*, 1999, Deng *et al.*, 2000a, Cappon *et al.*, 2000, etc.). A schematic drawing representing the different stages of the neck motion in a rear-end collision is shown in Figure 5. During a rear-end collision, as a consequence of forward acceleration of the vehicle the occupant is pushed forward by the seat back. This forces the thoracic spine to straighten up and as a result a vertical compressive force is observed in the neck. Owing to the inertia, the head lags behind and retracts during the forward motion of the torso (moves rearward without any angular motion) relative to the torso, see phase 1 in Figure 5. This results in an S-shaped curvature of the cervical spine. This is followed by a backward bending motion (extension) of the neck, see phase 2 and phase 3 in Figure 5. The maximum extension motion of the head and neck is determined by various factors such as severity of the impact, the design of the seat, the presence and position of a head restraint, along with physiological factors of the individual occupant.

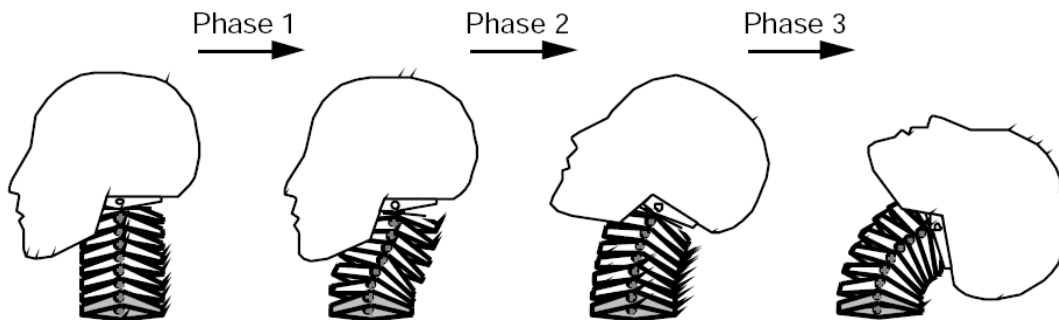


Figure 5 Schematic view of the whiplash motion (Svensson *et al.*, 1993)

1.3.2 Injury Mechanisms

To date, several hypotheses on injury mechanisms of whiplash injuries have been proposed. A shearing movement of the neck has been related to lesions of the facet joints, the combination of axial compressive force and posterior shear of the cervical spine causing a stretch of the facet joint capsule (Yang *et al.*, 1996). A study by Ono *et al.* (1997) suggests that pinching of a facet joint capsule takes place when it is trapped between the facet joint surfaces resulting in pain.

Svensson *et al.* (1993) suggested an injury mechanism due to transient pressure gradients in the spinal canal during the initial retraction phase causing ganglion damage. During the rapid motion of the whiplash, pressure gradients along the spinal canal and the intervertebral foramen are expected. These pressure gradients may arise due to two effects. The first one is the pressure gradient that occurs when a column of fluid accelerates and this pressure difference is proportional to the height of the fluid column as well as the magnitude of the acceleration. The second effect is the pressure gradient caused by the flow resistance in the vessels. These pressure gradients can be expected to result in injurious stresses and strains to the exposed tissues.

1.3.3 Injury Severity

Injury severity depends on various parameters in the case of rear-end impacts such as the mass and stiffness of the colliding objects and the delta-V (change in velocity) during the crash, the magnitude and duration of the acceleration pulse, the seat stiffness, the occupant seating posture and the position of the head restraint. An increased head to head restraint distance leads to larger extension of the neck, which is one of the reasons for neck injury symptoms. A study made by Jakobsson *et al.* (2000) suggests a trend towards an increased risk of injury if a pulse with high peak acceleration was judged to have occurred.

It has been suggested that the crash pulse produced in a car in a rear collision affects the injury outcome for the occupant (Kullgren *et al.*, 1999). According to the studies made by Thomson *et al.* (1993) and Parkin *et al.* (1995), stiffer and stronger seat backs, which were common during the 1990s, lead to higher risk of injury. However, when the seat back yields or collapses, the severity of the neck injury seems to decrease. Stother and James (1987) showed that the average seat back stiffness was 52 Nm/deg. More recently, Molino (1998) showed that the average seat back strength had increased to 65 Nm/deg. Based on an analysis of the NASS (National Accident Sampling Study) database and dummy sled tests, Prasad *et al.* (1997) concluded that stiffer seats could increase the incidence of minor and moderate neck injuries. They could also increase the loads to the thoracic and lumbar spine. The importance of seat design has also been highlighted by Svensson (1993), Walz and Muser (1995), Morris and Thomas (1996), Wiklund and Larsson (1998), Håland *et al.* (1996), Sekizuka (1998), Hofinger *et al.* (1999), Jakobsson and Norin (1999), Tencer *et al.* (2000) and Pike (2000), among others. Based on the fundamental mechanics of low velocity and centrally aligned direct impacts, Ray (2000) concludes that the delta-V of target vehicle and the acceleration in particular, are essential for the understanding of occupant acceleration and kinematics and hence the understanding of injury assessment. There are different kinds of acceleration pulses reported from tests with cars in rear impacts. Some publications (Krafft, 1998, and Zubay *et al.*, 1999) show

that the acceleration pulse can vary in both amplitude and duration for impacts of similar velocities.

Table 1 gives the Quebec classification of the whiplash injuries and the related symptoms. This table does not provide an option to include any assessment of the severity of the symptom. Implying that, suffering from intense pain with no other signs might be assessed as grade I, along with patient suffering from mild pain (Anderson *et al.*, 2006).

Table 1 Quebec classification of whiplash injuries

WAD grade	Clinical Representation (symptoms)
0	No neck complaint No physical sign(s)
I	Neck Pain Complaint Stiffness or Tenderness only
II	Neck Complaint Musculoskeletal sign (s), these include decreased range of motion and point tenderness
III	Neck pain Neurological Sign(s), these include decreased or absent deep tendon reflexes, weakness and sensory deficits
IV	Neck complaint Fracture or dislocation

1.4 Neck Injury Criterion and Tolerance Levels

Injury criteria form an important basis for evaluating a safety system. An injury criterion relates to a physical variable in the occupant to a specific injury. Based on the tolerance level for human tissue, an injury criterion level is chosen beyond which an injury occurs.

NIC (Neck Injury Criterion) was proposed by Boström *et al.* in 1996. It is probably the most widely used criteria to assess low-intensity neck loading. NIC is a value that relates the movement of the head relative to the base of the neck (T1 vertebra). It assumes pressure aberrations inside the cervical fluid compartments that occur due to

a swift extension-flexion motion (S-shape) in the early stages of a rear-end impact (Svensson *et al.*, 1993). NIC is calculated using equation (1.1).

$$NIC = 0.2 \cdot (T_{1Accel} - Head_{CgAccel}) + \left[\int (T_{1Accel} - Head_{CgAccel}) dt \right]^2 \quad (1.1)$$

T_{1Accel} is the acceleration at T1 vertebra and $Head_{CgAccel}$ is the acceleration at the center of gravity of the head. Though this criterion is dimensionally unstable it is widely accepted to measure the injury risk.

The NIC is intended to be calculated at maximum retraction. The tolerance level for NIC is $15 \text{ m}^2/\text{s}^2$ beyond which an occupant is most likely to be injured.

1.5 Facet Joint Capsule Strain

As discussed in Section 1.3.2, pinching of a facet joint capsule takes place when it is trapped between the facet joint surfaces resulting in pain. This facet joint strain is correlated to the relative displacements of the vertebrae (Kitagawa *et al.*, 2006). Winkelstein *et al.* (1999) examined the deformation of the joint capsules related to the relative motion between adjacent vertebrae.

Siegmund *et al.* (2000) conducted quasi-static loading tests on C3-C4 components of PMHS (Post Mortem Human Subject) by subjecting them to shear and compressive loadings, see Figure 6. The anterior-posterior displacement and the sagittal rotation of C3 with respect to C4 were monitored. Joint capsule strain was estimated from relative displacement of the photo markers posted to the capsule tissue. In this work the facet joint strains are calculated by applying similar boundary conditions to the THUMS model. The anterior-posterior displacement and sagittal rotations are calculated from nodal displacements in the model and joint capsule strain is directly obtained from the elements forming the capsule tissues.

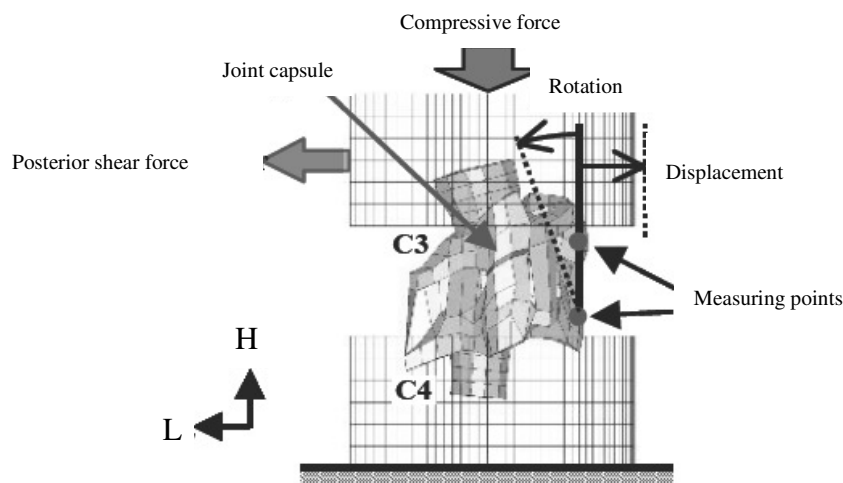


Figure 6 Loading test C3, C4 Vertebrae (Siegmund *et al.*, 2000)

1.6 Objective

Facet joint loadings (Yang *et al.*, 1996 and Yoganandan *et al.*, 2001) and pressure transients (Svensson *et al.*, 1993) in the spinal canal are hypothesized to be potential causes for the severe neck injury symptoms in rear-end impacts, as mentioned in Section 1.3.2. The objective of this study is to investigate how facet joint loadings and pressure gradients are affected by different acceleration pulses, head restraint and its position and different seating postures.

The study is divided into the following steps:

- Perform FE simulations of the THUMS model in a variety of crash pulses and conditions that are known to influence risk of long term injuries to analyse facet joint loadings and neck injury criterion (NIC).
- Model the whiplash motion with OpenFOAM using the motion output from FE simulations and by applying it in the geometrical model. The pressure gradients are then investigated performing CFD simulations.

2 Methodology

The study is divided into different parts consisting of the definition of the acceleration pulses and the parametric matrix for which the FE and the CFD simulations are performed. This section also includes the steps followed in the FE and the CFD modelling.

2.1 FE Modelling

The FE modelling focuses on the two models used for the simulations, THUMS which mimics the human body and the driver seat model where the THUMS is seated.

2.1.1 THUMS

The study utilizes a human body FE model named Total HUMAN Model for Safety (THUMS, see Figure 7), which was jointly developed by Toyota Motor Corporation and Toyota Central Research and Development Laboratory. THUMS represents an average-sized adult male (175 cm and 77 kg). The model includes approximately 60,000 nodes and 80,000 elements, and it runs on the commercial finite element code LS-DYNA™ (Hallquist, 2007).

The THUMS model replicates human body kinematics during car crashes. It incorporates joint modelling, all the bony parts and major ligaments for simulating a real human subject. The modelling of ligaments is made by connecting bones to bones and contacts are also defined between them. This modelling method simulates realistic joint motions and calculates force transmission through the joint. Different body parts of THUMS are modelled to represent the human tissue material in terms of mechanical response against external loading.

The model also incorporates several internal organs, skin, fat, muscle, brain etc. and most of them are modelled as solid parts in THUMS. The neck muscles are modelled with 1D discrete element to simulate their passive responses against stretch. The cervical facet joint capsules in the model enable in calculating joint capsule strain. The THUMS model has a detailed representation of the neck vertebrae which is shown in Figure 7.

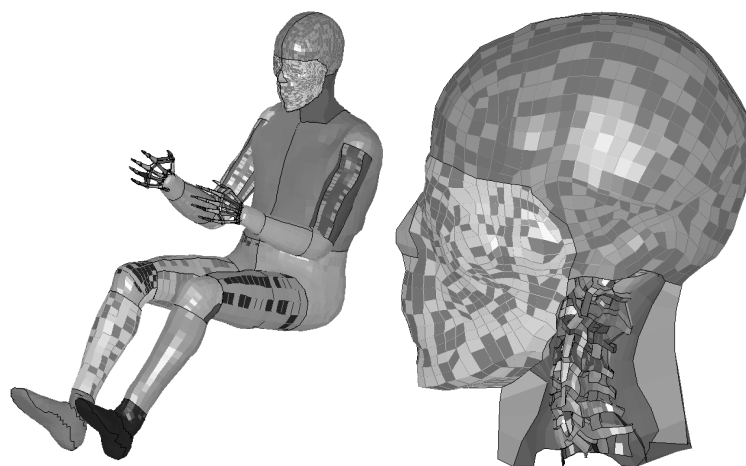


Figure 7 THUMS (left), detailed neck modelling (right)

2.1.2 Driver Seat

The study utilizes a driver seat which is extracted from the FE model of Ford Taurus (model: 2001) by NCAC (FWHTSA/NHTSA, National Crash Analysis Center), see Figure 8. This model has been validated for frontal impacts.

The seat is a simplified model with head restraint and without seat belt. The lower and back cushions of the seat have single uniform stiffness throughout. Since the model was validated only for frontal impacts, the extracted model of the seat is modified to suit for the rear-end impacts. The initial model has a relatively stiff back rest and fails to represent a real seat back deflection for the rear-end crash simulations. Hence a revolute joint is added into the model to incorporate seat back deflection. The stiffness values for the joint and seat back deflection angles are obtained from the research papers (Eriksson, 2004). The seat is also added with required constraints and contacts. To have better contact definition between the seat and THUMS, shell elements with null material are created on the outer surfaces of the head restraints, seat lower and back cushions.

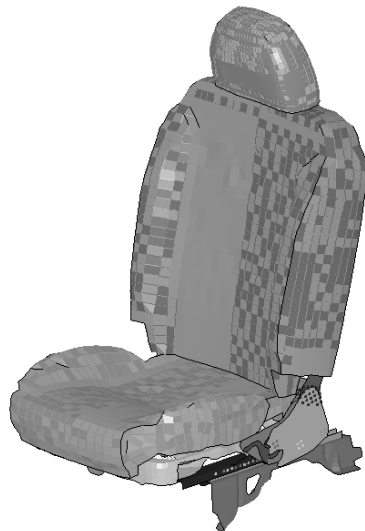


Figure 8 Driver seat

2.2 Crash Pulses

Studies have shown that the peak accelerations of a crash pulse for a given delta-V produced in the car during rear-end collision has considerable effect on the severity of the injury outcome (Kullgren *et al.*, 1999). Hence the study in this work is made utilizing crash pulses with different magnitudes of peak accelerations (2.5g, 5g and 7.5g). All the above mentioned crash pulses are modelled for delta-V of 15 km/h.

The different magnitudes of pulses selected for this study cover a wide range of injury outcomes which includes a pulse that causes no injury to the occupant (2.5g) and pulses that are probable to cause medium to severe injuries to the occupant (5g and 7.5g, respectively) during rear-end collisions. The crash pulses used in this study are represented in Figure 9.

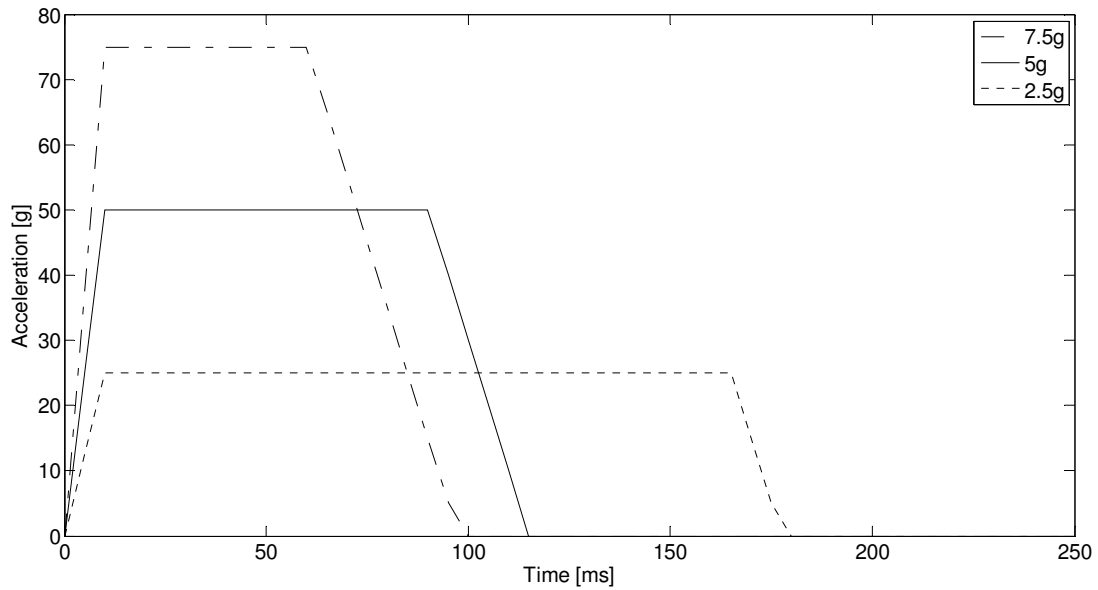


Figure 9 Square crash pulses at delta-V of 15 km/h used in this study

2.3 Parametric Study

Since real crashes have multiple configurations depending on the crash conditions an effort is made to study the possible conditions of crashes. The effect of presence and absence of head restraint, position of head restraint and incorrect posture on severity of the injury outcome is studied for different variety of crash pulses. All the crash pulses used in the study correspond to a delta-V of 15 km/h. The configurations chosen (X) for the study are presented in Table 2.

Table 2 Configurations used for the study

	With Head Restraint	Without Head Restraint	Varied Head Restraint Position (7 cm from the head)	Non-Upright Posture
2.5g	X	X		
5g	X	X		
7.5g	X	X	X	X

2.4 CFD Modelling of the Venous Plexus

The venous plexus surrounding the spinal canal is the network of blood vessels where the pressure changes due to the whiplash motion cause injuries in the nerves. The purpose is to solve these pressure gradients and hence the venous plexus, considering its physical behaviour, and the whiplash motion tracked in the FE simulations are modelled.

2.4.1 Theoretical Model

The spinal canal is located in the vertebral column, therefore the length of the cervical spinal canal changes during the whiplash motion. It decreases during extension and increases during flexion (Breig, 1978). The cross-sectional area of the cervical spinal canal also decreases during the extension of the neck due to the protrusion of the ligament flava into the canal (Breig, 1978), see Figure 10. Therefore, the inner volume of the spinal canal decreases during the neck extension and increases during the flexion. However, all the tissues and fluids (fat, blood and Cerebro Spinal Fluid – CSF) inside the spinal canal are virtually incompressible (Estes and McElhaney, 1971). Considering that the CSF flow is of minor importance for the volume compensation, blood transportation through the spinal canal must take place to compensate the volume change caused by the whiplash motion (Svensson *et al.*, 1993). As whiplash motion is a rapid motion, the venous blood speed is changed rapidly and significant pressure gradients are generated along the intervertebral foramen. These gradients are thought to be the indirect cause of the injuries because they are expected to increase the shear stress in the soft tissues.

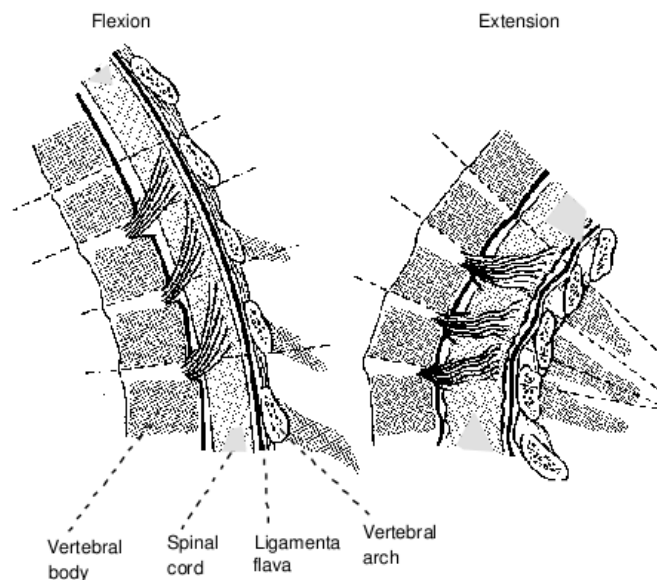


Figure 10 A sagittal cross-section of the lower cervical spine where flexion and extension are shown (Svensson, 1993)

The pressure magnitude at each level of the cervical spine depends on the velocity and acceleration of the change of the inner volume of the spinal canal. Therefore, the velocity of volume change can be used as an indicator for injury risk in simulations of low-speed rear-end impacts.

2.4.2 Geometrical Modelling

The main hypothesis is that the whiplash motion of the neck results in pressure gradients in blood flowing through the venous plexus. Hence, in this study, the network of blood vessels (spinal venous plexus) surrounding the spinal cord is modelled with respect to THUMS model, as shown in Figure 11.

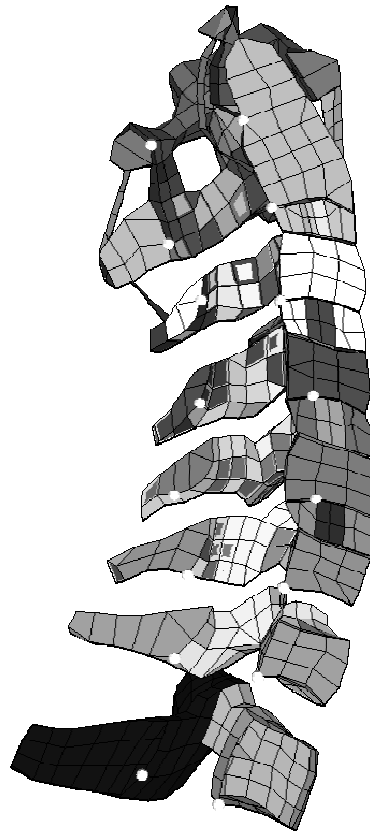


Figure 11 Lateral view of the cervical vertebrae from the THUMS model with its representative nodes (white dots)

The network of blood vessels is simplified as a hollow cylinder which represents a unique blood vessel that surrounds the spinal cord. Figure 12 a and b show frontal and lateral view of the model in the initial straight position, respectively. Figure 12 c shows the modification of this initial position of the venous plexus (Figure 12 b) to the corresponding initial position in the THUMS model (see Figure 11). The geometry is created as a straight pipe since it is easier having a straight geometry as a reference position; this is explained in Section 2.4.3.

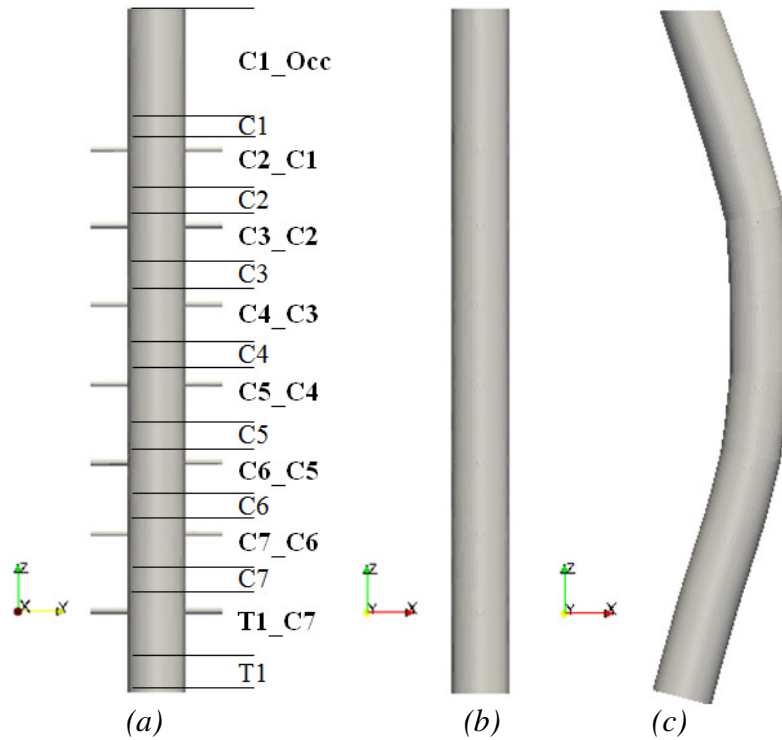


Figure 12 Views of the geometrical model of the venous plexus; frontal view (a), lateral view (b and c)

In the current model, the pipe is divided into different cylinders which represent the different zones of the vertebral and intervertebral bodies. These zones are non-deformable and deformable cylinders, respectively, and they are named according to which body they represent, see Figure 12 a, where the names in bold represent the naming of the deformable cylinders and the others represent the rigid cylinders.

It is assumed that the height of the rigid cylinder is half of the original height of the vertebral body obtained in THUMS, see scheme in Figure 13. Therefore, the height of the deformable cylinders is the sum of the second half of the vertebral body and the original height of the intervertebral bodies. The purpose of this assumption is that the deformation of only a part of the blood vessels network located at the inner part of the vertebrae is negligible. In addition, the blood vessels going out from the main vertical vessels network in a transversal direction are modelled by side pipes connected to the deformable cylinders.

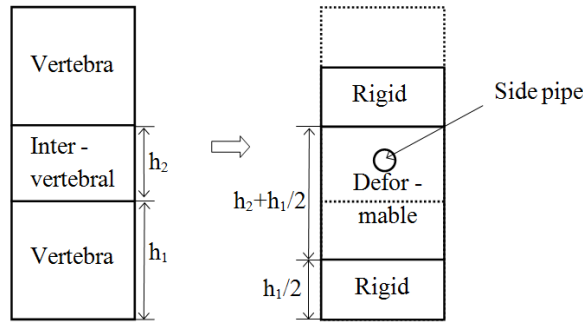


Figure 13 Scheme of the cylinder heights from THUMS (left) and the modelled ones (right)

Since the motion data is obtained from THUMS, the heights of the vertebral and intervertebral bodies, which define the heights of the different cylinders, are measured from the THUMS. The geometry definitions are shown in Table 3, where the accumulated cylinder height is also added to describe the total height of the model used in the study.

Table 3 Heights of the vertebral and intervertebral bodies and their respective modelled cylinders (bold names represent the deformable cylinders)

Part	Measured height [mm]	Cylinder height [mm]	Accumulated cylinder height [mm]
C1_Occ	21.9	25.8	160.1
C1	7.7	3.9	134.3
C2_C1	6.6	12.5	130.4
C2	11.9	5.9	117.9
C3_C2	5.2	11.4	112.0
C3	12.5	6.2	100.5
C4_C3	6.8	12.6	94.3
C4	11.6	5.8	81.6
C5_C4	6.9	13.1	75.8
C5	12.3	6.1	62.8
C6_C5	5.3	10.7	56.6
C6	10.8	5.4	45.9
C7_C6	6.4	11.9	40.5
C7	10.8	5.4	28.6
T1_C7	7.9	15.5	23.2
T1	15.4	7.7	7.7

Figure 14 shows the top view of the hollow cylinder. The external diameter of this cylinder is equal to the diameter of the spinal canal, which is 13.73 mm (Morishita *et al.*, 2008). The intervertebral veins, which pass through the intervertebral foramen in transversal direction, connect the internal venous plexus to the external venous plexus. These intervertebral veins, referred as side pipes, are assumed to be located one at each side of the main pipe and at 90° with respect to the vertical and main pipe.

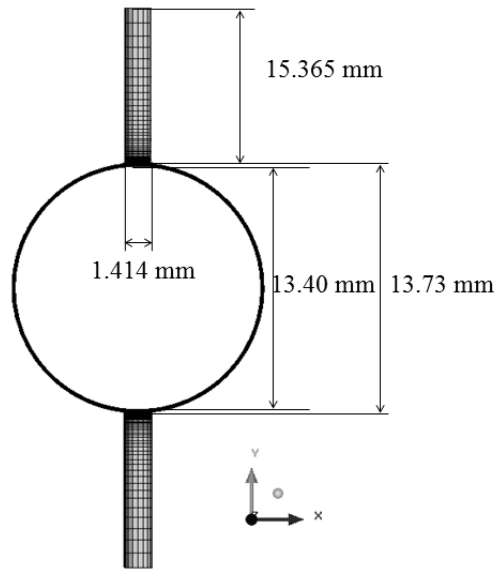


Figure 14 Superior view of the geometrical model of the venous plexus

The cross-sectional area of the pipe modelling the blood vessels considers the sum of the cross-sectional areas of blood veins forming this network, which is $\pi \cdot 1.5^2 \text{ mm}^2$, and the total cross sectional area of the side pipes is $\pi \cdot 1^2 \text{ mm}^2$ (Clemens, 1961 and Liu and Yang, 2008). This information is used to calculate the inner diameter of the cylindrical pipe and the diameter of the side pipes, see Figure 12. The inner diameter is 13.40 mm, see equation (3.1).

$$\pi \cdot 1.5^2 = \pi \cdot (13.73/2)^2 - \pi \cdot r_{\text{inner}}^2 \rightarrow r_{\text{inner}} = 6.70 \text{ mm} \rightarrow \phi_{\text{inner}} = 13.40 \text{ mm} \quad (3.1)$$

where 13.73 mm is the outer diameter.

The diameter of the side pipes is 1.414 mm, see equation (3.2).

$$\pi \cdot 1^2 = 2 \cdot \pi \cdot r^2 \rightarrow r = 0.707 \text{ mm} \rightarrow \phi = 1.414 \text{ mm} \quad (3.2)$$

The length of the side pipes is 15.365 mm based on Liu and Yang study (2008).

The geometry and the block-structured mesh of the model described are created with ICEM CFD, a CAD and mesh generation software (see Figure 15). This mesh consists of 142224 hexahedra.

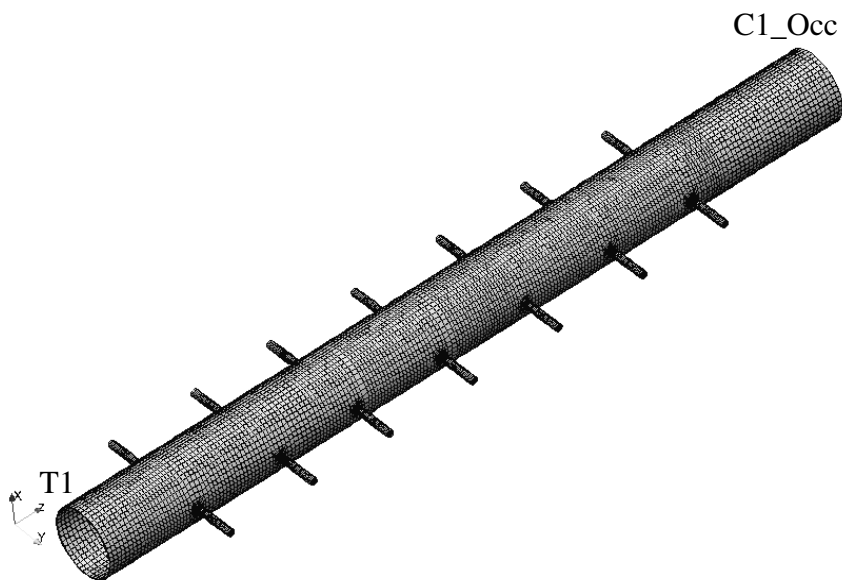


Figure 15 View of the whole mesh before adopting the initial shape

The mesh is as uniform as possible along the different cylinders and it is refined at critical zones where sharp edges and difference in thicknesses are seen; these critical zones are the regions where the side pipes are connected to the main cylinders, see Figure 16.

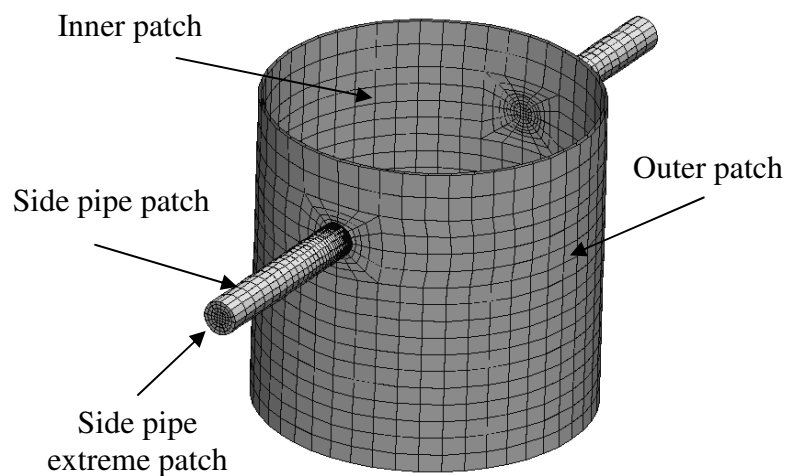


Figure 16 Intervertebral body between C4 and C5 before adopting the initial shape

To ensure the possibility of defining the boundary conditions with ease, the model is defined into different patches, see Figure 16. These patches include

- The uppermost and the lowermost surfaces which delimits the whole cylindrical model, in C1_Occ and T1, respectively.
- The inner and outer surface of each cylinder.
- The side pipe's walls.
- The side pipe's extremes.

2.4.3 Kinematic Modelling

From the data of the whiplash motion of the THUMS, the positions and displacements of representative nodes (see the white dots in Figure 11) are exported in each time step. These representative nodes are located at the anterior and posterior part of each lowest circumference of the modelled rigid cylinders. By interpolation of the nodal information of these pairs of nodes selected in THUMS, the motion information of the center points of the circumferences located in the lowest surface of each rigid cylinder (named representative points, see Figure 17) is calculated. This information is input for the kinematic model of the blood vessels network done in OpenFOAM.

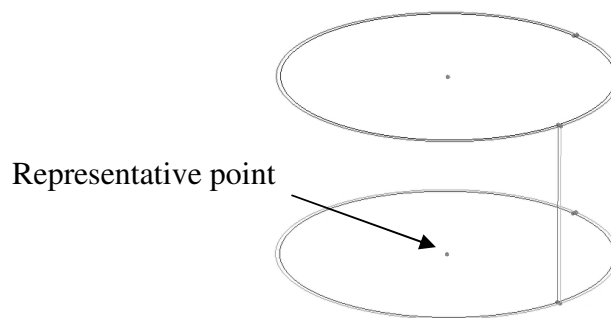


Figure 17 Scheme of one vertebral body and its representative point

The input data to model the motion of the blood vessels are:

- Position of the representative points and heights of the different cylinders from the reference geometry, which represents the cylinders without any orientation as shown in Figure 12.
- Information (position and orientation) of the representative points at the initial position of the cylinders in THUMS.
- Motion (translation and rotation) from the reference geometry to obtain the initial position of the cylinders in THUMS, which is shown in Figure 12.
- Motion (translation and rotation) of the representative points.

The kinematic model has been coded in OpenFOAM by defining a new class. This model has the following parts:

- I. Reading input data and saving it in matrices.
- II. Calculation of the motion for each cylinder, taking into account that the motion for the rigid cylinders and the deformable ones are calculated in different ways:
 - For the rigid cylinders, the rotation and translation is directly applied with respect to the representative point of each cylinder. The motion is modelled in two steps; initially the cylinders are moved from the reference geometry to initial position of the cylinders in THUMS, named premotion.

And with respect to this position, the motion data from the FE simulations during the rear-end impact is added, called motion. Knowing the position, orientation, translational and rotational motion of the representative points, the rigid cylinders can be moved extrapolating this motion information to all the points of the rigid cylinders and using the 3D matrix of rotation (see equation (3.3)) to get the translation for both steps in this motion (premotion and motion), see equation (3.4) and (3.5).

$$R = R_\gamma \cdot R_\theta \cdot R_\varphi = \begin{pmatrix} \cos \gamma & -\sin \gamma & 0 \\ \sin \gamma & \cos \gamma & 0 \\ 0 & 0 & 1 \end{pmatrix} \begin{pmatrix} \cos \theta & 0 & -\sin \theta \\ 0 & 1 & 0 \\ \sin \theta & 0 & \cos \theta \end{pmatrix} \begin{pmatrix} 1 & 0 & 0 \\ 0 & \cos \varphi & -\sin \varphi \\ 0 & \sin \varphi & \cos \varphi \end{pmatrix} \rightarrow$$

$$R = \begin{pmatrix} \cos \gamma \cdot \cos \theta & -\sin \gamma \cdot \cos \varphi - \cos \gamma \cdot \sin \theta \cdot \sin \varphi & \sin \gamma \cdot \sin \varphi - \cos \gamma \cdot \sin \theta \cdot \cos \varphi \\ \sin \gamma \cdot \cos \theta & \cos \theta \cdot \cos \varphi - \sin \gamma \cdot \sin \theta \cdot \sin \varphi & -\cos \gamma \cdot \sin \varphi - \sin \gamma \cdot \sin \theta \cdot \cos \varphi \\ \sin \theta & \cos \theta \cdot \sin \varphi & \cos \theta \cdot \cos \varphi \end{pmatrix} \quad (3.3)$$

In equation (3.3), R is the 3D matrix of rotation and φ , θ , γ are the rotations about X, Y, Z respectively.

$$\begin{pmatrix} X_{premoved} \\ Y_{premoved} \\ Z_{premoved} \end{pmatrix} = R_{premotion} \cdot \begin{pmatrix} X - X_{ref0} \\ Y - Y_{ref0} \\ Z - Z_{ref0} \end{pmatrix} + \begin{pmatrix} \Delta X_{premotion} \\ \Delta Y_{premotion} \\ \Delta Z_{premotion} \end{pmatrix} + \begin{pmatrix} X_{ref0} \\ Y_{ref0} \\ Z_{ref0} \end{pmatrix} \quad (3.4)$$

$$\begin{pmatrix} X_{moved} \\ Y_{moved} \\ Z_{moved} \end{pmatrix} = R_{motion} \cdot \begin{pmatrix} X_{premoved} - X_{ref} \\ Y_{premoved} - Y_{ref} \\ Z_{premoved} - Z_{ref} \end{pmatrix} + \begin{pmatrix} \Delta X_{motion} \\ \Delta Y_{motion} \\ \Delta Z_{motion} \end{pmatrix} + \begin{pmatrix} X_{ref} \\ Y_{ref} \\ Z_{ref} \end{pmatrix} \quad (3.5)$$

In equation (3.4), $_{ref0}$ refers to the position of the representative points in the reference position and, in equation (3.5), $_{ref}$ refers to the position of the same points in the initial position of the THUMS.

- The motion of the deformable cylinders is achieved by interpolation of the rigid cylinders motion. For each point of the deformable cylinders, its projection on the upper and lower rigid cylinders are calculated. The motion from these points is extrapolated from the representative point's motion of their respective rigid cylinders. Using equations (3.4) and (3.5) for the upper projected point and the lower one, the new coordinates of the projected points are calculated. Subtracting their initial positions, their translations are obtained. According to the distances between the projected points and the deformable cylinder point that is being moved (see Figure 18), the interpolation weights to find out the proportional motion are calculated; see equations (3.6) and (3.7).

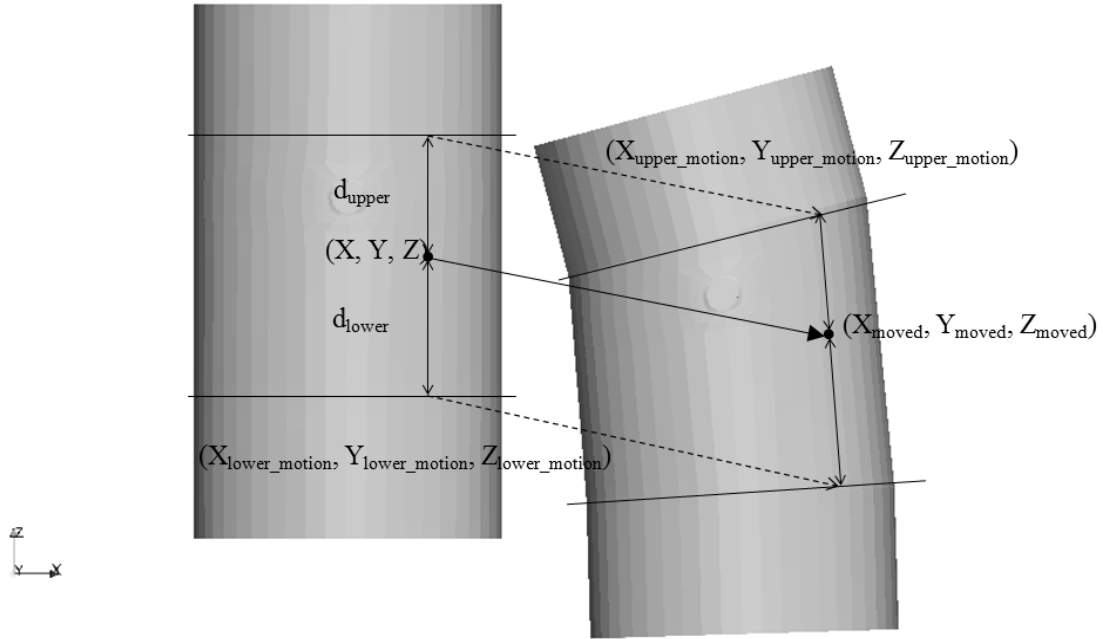


Figure 18 Motion from initial LS-DYNA layout until $t = 20$ ms

$$\begin{pmatrix} X_{upper_motion} \\ Y_{upper_motion} \\ Z_{upper_motion} \end{pmatrix} = \begin{pmatrix} X_{upper_moved} \\ Y_{upper_moved} \\ Z_{upper_moved} \end{pmatrix} - \begin{pmatrix} X_{upper} \\ Y_{upper} \\ Z_{upper} \end{pmatrix} \quad (3.6a)$$

$$\begin{pmatrix} X_{lower_motion} \\ Y_{lower_motion} \\ Z_{lower_motion} \end{pmatrix} = \begin{pmatrix} X_{lower_moved} \\ Y_{lower_moved} \\ Z_{lower_moved} \end{pmatrix} - \begin{pmatrix} X_{lower} \\ Y_{lower} \\ Z_{lower} \end{pmatrix} \quad (3.6b)$$

$$d_{upper} = Z_{upper} - Z \quad (3.7a)$$

$$d_{lower} = Z - Z_{lower} \quad (3.7b)$$

$$d_{total} = d_{upper} + d_{lower} \quad (3.7c)$$

$$weight_{upper} = (d_{total} - d_{upper}) / d_{total} \quad (3.7d)$$

$$weight_{lower} = (d_{total} - d_{lower}) / d_{total} \quad (3.7e)$$

Then, using the weights and the motion of the projected points, the interpolated motions for the points from the intervertebral cylinders are calculated as shown in equation (3.8).

$$\begin{pmatrix} X_{int\ erpolated_motion} \\ Y_{int\ erpolated_motion} \\ Z_{int\ erpolated_motion} \end{pmatrix} = \begin{pmatrix} X_{upper_motion} \\ Y_{upper_motion} \\ Z_{upper_motion} \end{pmatrix} \cdot weight_{upper} + \begin{pmatrix} X_{lower_motion} \\ Y_{lower_motion} \\ Z_{lower_motion} \end{pmatrix} \cdot weight_{lower} \quad (3.8)$$

Finally, the moved coordinates of each point located in the deformable cylinders are calculated by adding the interpolated motion to their initial coordinates, shown in equation (3.9).

$$\begin{pmatrix} X_{moved} \\ Y_{moved} \\ Z_{moved} \end{pmatrix} = \begin{pmatrix} X_{int\ erpolated_motion} \\ Y_{int\ erpolated_motion} \\ Z_{int\ erpolated_motion} \end{pmatrix} + \begin{pmatrix} X \\ Y \\ Z \end{pmatrix} \quad (3.9)$$

2.4.4 Definition of the Fluid Dynamic Properties

The blood flow is considered to be laminar because it is not expected to have Reynolds numbers (Re) above the laminar to turbulent threshold, defined as 2300. Re is based on the kinematic viscosity (ν), the speed (U) and the width (h) through which the blood flows, see equation (3.10). The blood is considered as a Newtonian fluid, which means that its viscosity is not depending on the forces acting on it, it just depends on temperature and pressure. And its main properties are presented in Table 4.

$$Re = \frac{U \cdot h}{\nu} = \frac{U \cdot 1.65 \cdot 10^{-4}}{3.33 \cdot 10^{-6}} < 2300 \quad (3.10)$$

Table 4 Blood properties (Mukhin et al., 2006)

Property	Value
density, ρ [kg/m ³]	1050
dynamic viscosity, μ [kg/ms]	0.0035
kinematic viscosity, ν [m ² /s]	$3.33 \cdot 10^{-6}$

Compressibility for the blood is defined considering the flexibility of the veins. This compressibility is defined by the Bulk modulus and its value is $6.13 \cdot 10^5$ Pa (Cedric, 2008).

Referring to boundary conditions, since blood flows through the bottom part of the spinal cord, as well as to the brain, the flow must be able to get in and out of the modelled pipe. Therefore, the extremes of the main pipe as well as the side exits are considered as inlets and outlets to permit the blood to flow. The boundary conditions for the rest of the model are defined as walls, which cannot be penetrated.

Concerning the velocity conditions:

- Inlets/outlets have Neumann condition, where the velocity gradient is set to zero.
- The rest of the walls and the mesh take the velocity given by the kinematic model.

Concerning the pressure conditions:

- Inlets/outlets have Dirichlet condition by defining the fixed mean value of pressure equal to zero.
- For the rest, the pressure gradient is set to zero.

2.4.5 Solver and Numerical Schemes

The fluid dynamic problem to be solved consists of a laminar flow of a newtonian fluid which flows through a deforming canal in motion. The pressure and velocity fields are solved by using the Continuity equation and the Navier-Stokes equations (momentum equation):

$$\frac{\partial \rho}{\partial t} + \frac{\partial \rho U_i}{\partial x_i} = 0 \quad (3.11)$$

$$\frac{\partial \rho U_i}{\partial t} + \frac{\partial}{\partial x_j} (\rho U_i U_j) = - \left(\frac{\partial P}{\partial x_i} \right) + \mu \frac{\partial^2 U_i}{\partial x_j \partial x_j} \quad (3.12)$$

where ρ is the blood density, U_i is the velocity, P is the pressure and μ is the dynamic viscosity.

In the initial simulation, the blood is considered incompressible, for which the *icoDyMFoam* solver is used. This is a transient solver for incompressible, laminar flow of newtonian fluids with dynamic mesh. The *icoDyMFoam* solver uses the Pressure-Implicit Split-Operator algorithm (PISO), which is an iterative pressure-velocity coupling procedure. By guessing some initial values of pressure (P^*), the discretized momentum equations are solved to get the velocity components (U^* , V^* and W^*), which will not satisfy the continuity equation unless the pressure field guessed initially is correct. Then, the first corrector step is introduced to give a velocity field (U^{**} , V^{**} and W^{**}), which satisfies the discretized continuity equation. So a pressure corrector field (P') is introduced and then the corrected velocity fields (U^{**} , V^{**} and W^{**}) are calculated using equations (3.14 a-d).

$$P^{**} = P^* + P' \quad (3.14a)$$

$$U^{**} = U^* + U' \quad (3.14b)$$

$$V^{**} = V^* + V' \quad (3.14c)$$

$$W^{**} = W^* + W' \quad (3.14d)$$

This corrector step is repeated as many times as correctors are defined and at the last step, the pressure field (P^{n*}) and the velocity fields (U^{n*} , V^{n*} and W^{n*}) are considered to be the correct solution (P , U , V and W).

A similar solver but based on the Semi-Implicit Method for Pressure-Linked Equations algorithm (SIMPLE) is also used, which is called *icoDyMSimpleFoam*. It is a guess-and-correct procedure for the calculation of pressure-velocity coupled equations. This procedure evaluates also an initial guessed solution and then by correction the solution is reached. But the pressure correction equation is susceptible to divergence unless some under-relaxation is used during the iterative process, and new, improved, pressures field (p^{new}) are obtained, see equation (3.15):

$$p^{new} = p^* + \alpha \cdot p' \quad (3.15)$$

where α is the under-relaxation factor (if equal to zero there will not be correction at all). The velocities are also under-relaxed. Too large value of α may lead to oscillatory or even divergent iterative solutions, and a value which is too small will cause extremely slow convergence. Considering that, the under-relaxation factor taken for pressure is 0.3 and 0.7 for velocities.

The main differences between the PISO and SIMPLE algorithms are that the SIMPLE algorithm adds the under-relaxation factors and introduces coupled iterations within each time step. This implies that the equations of pressure and velocity are being solved iteratively together. In the PISO-based solver, the coupling is more explicit, which has shown to be unstable for skewed meshes and large time steps.

The development of a solver to consider blood as a compressible fluid is also carried out. This solver is called *sonicLiquidFoamMeshMotion* and it is based on the *sonicLiquidFoam* solver, a transient solver for trans-sonic/supersonic, laminar flow of a compressible liquid. This solver is modified to add to it the mesh motion feature. This solver is based on the PISO algorithm.

The solvers are modified to not compute the velocities and pressures during the initial motion of the cylinders, which is the motion from the reference position to the initial position in THUMS. With this modification, the influence of this initial motion in the results is avoided.

The interpolation scheme used for the convection term is the upwind scheme which takes into account the flow direction. For the other terms of the equations to solve, equations (3.11) and (3.12), the interpolation scheme used is the central differencing scheme, which is a linear interpolation. In the case of the first time derivative scheme ($\partial / \partial t$), the Euler scheme is used, which is a first-order, bounded and implicit time scheme.

3 Results and Discussions

The output from the FE and CFD simulations are analysed and discussed to understand the parameters affecting the injury outcome are discussed in the following sections.

3.1 Motion

As mentioned in Table 2, eight simulations with different configurations are carried out with the THUMS model. Since all the configurations show similar trends, an analysis of the configuration of 5g acceleration pulse with head restraint is carried out in this section.

Figure 19 shows the angle of the different vertebra around the Y axis (transversal to the acceleration pulse direction) obtained from FE simulations. In the first phase of the motion, all the vertebrae rotate in negative direction because head rotates backwards. The largest rotation is taking place in the uppermost vertebrae (C1) and the smallest rotation in the lowermost vertebrae (T1). At about 0.115 s, the rotational displacements of all the vertebrae reach the maximum value, between -9.6 (T1) and -14.3 deg (C1); this defines the point of maximum extension.

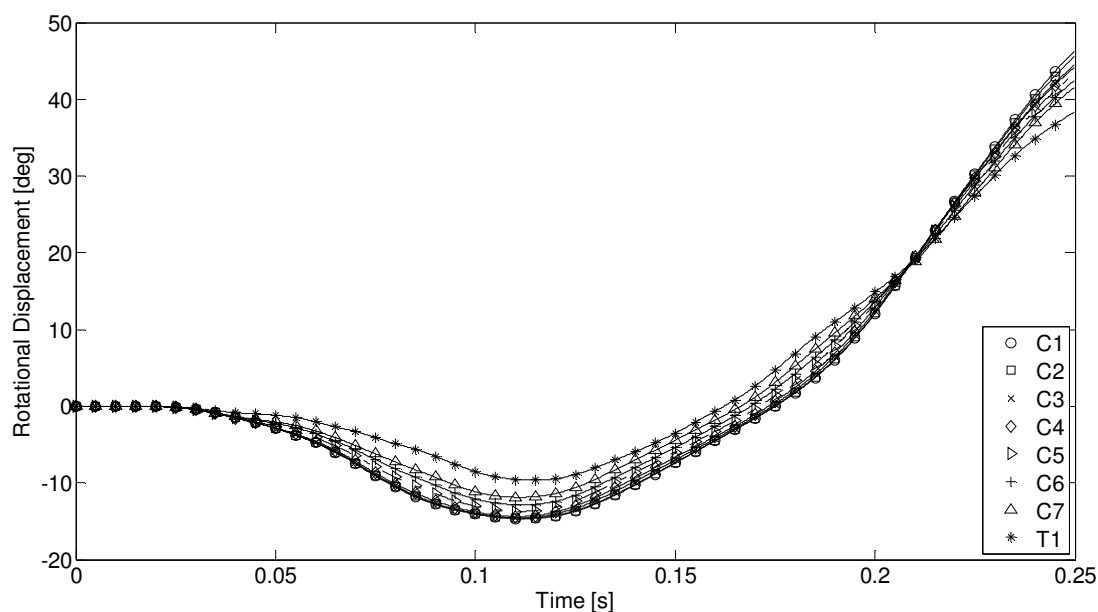


Figure 19 Rotational displacement of the different vertebrae

Figure 20 shows the longitudinal acceleration of the different vertebra and it is observed that the maximum acceleration is at about 0.115 s where the maximum extension is occurring. Afterwards, the acceleration of all the vertebrae decreases and even it turns to be negative at around 0.16 s.

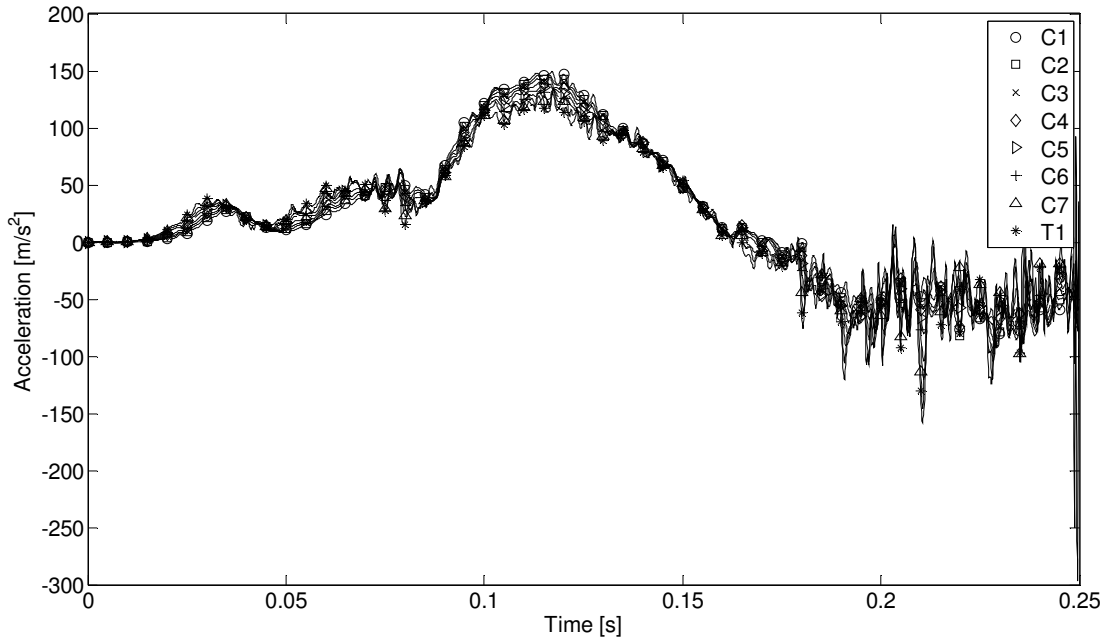


Figure 20 Longitudinal acceleration of the different vertebra

This whiplash motion is exported from FE simulation and imported to a new library in OpenFOAM. This motion is verified with the motion from FE simulation for the configuration consisting of 5g of acceleration and with head restraint. Figure 21, Figure 22 and Figure 23 show that the three components of velocity for the FE and CFD models match.

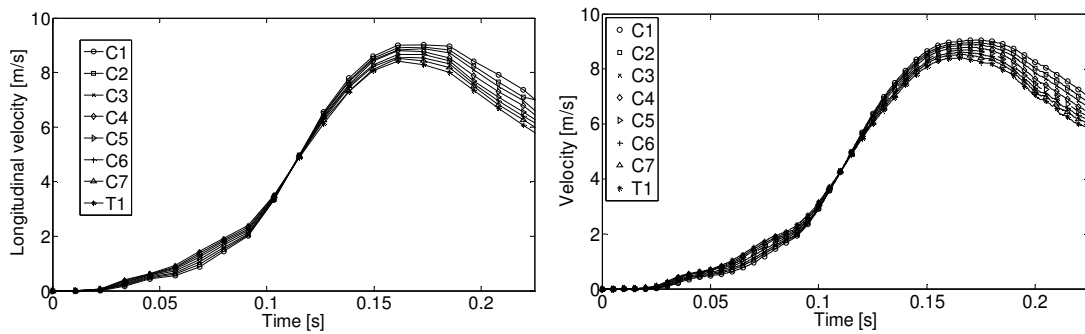


Figure 21 Longitudinal velocity of the different vertebrae from OpenFOAM (left) and THUMS (right)

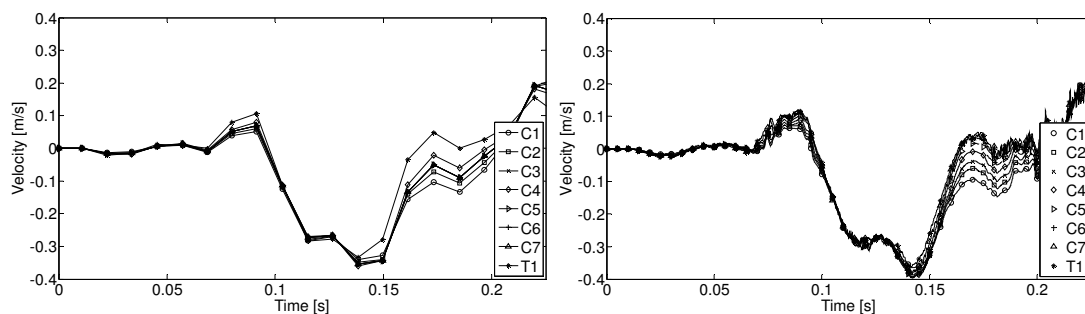


Figure 22 Lateral velocity of the different vertebrae from OpenFOAM (left) and THUMS (right)

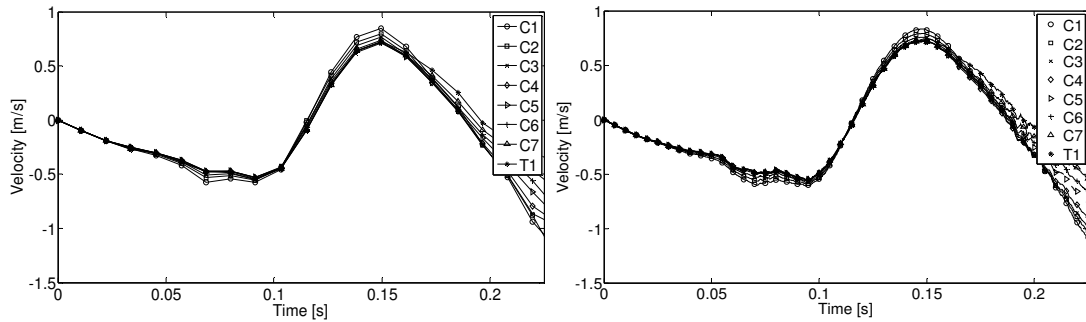


Figure 23 Vertical velocity of the different vertebrae from OpenFOAM (left) and THUMS (right)

Observing the figures for velocities (Figure 21, 22 and 23), the motion mainly takes place in the longitudinal direction, which is the direction in which the acceleration pulse is applied. Observing Figure 21, the longitudinal speed increases until a maximum at about 0.16 s with values in between 8.3 and 9 m/s. The upper vertebrae have larger velocities compared to the lower vertebrae. The lateral speed of the vertebrae is rather small and hence can be neglected, see Figure 22. In Figure 23, it is observed that the vertical velocity of the vertebrae has a negative magnitude between 0 and 0.115 s, point of maximum extension. This motion is due to the energy absorption of the cushion of the seat. Afterwards, the model rebounds and it moves upwards.

The motion for this configuration is also shown in Figures 24, 25 and 26. The longitudinal displacement between time steps in the beginning of the simulation is smaller compared to the time steps towards the end, due to the increase of longitudinal speed with time shown in Figure 21. Apart from the main motion in the longitudinal direction, there is some motion in the vertical direction, as mentioned previously.

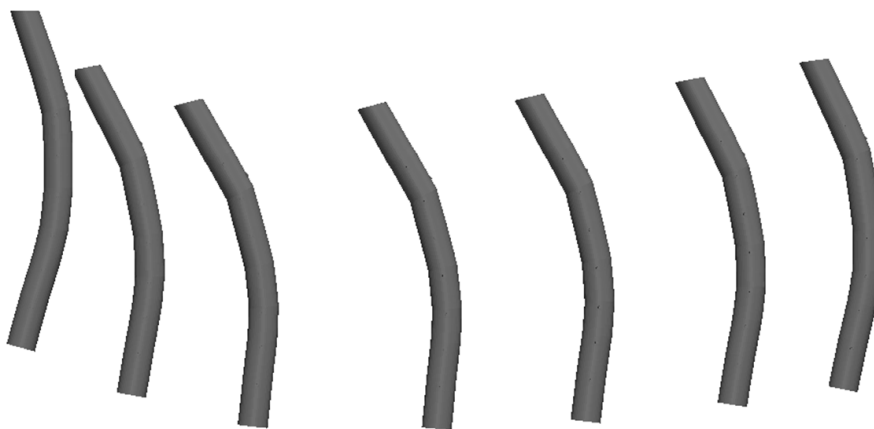


Figure 24 Position and shape of the model at $t = 0, 0.08, 0.10, 0.12, 0.13, 0.14$ and 0.15 s, respectively

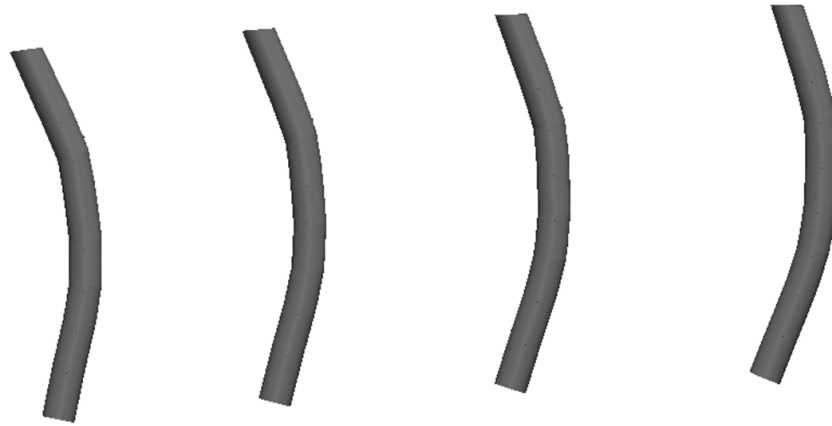


Figure 25 Position and shape of the model at $t = 0.15, 0.16, 0.17$ and 0.18 s, respectively

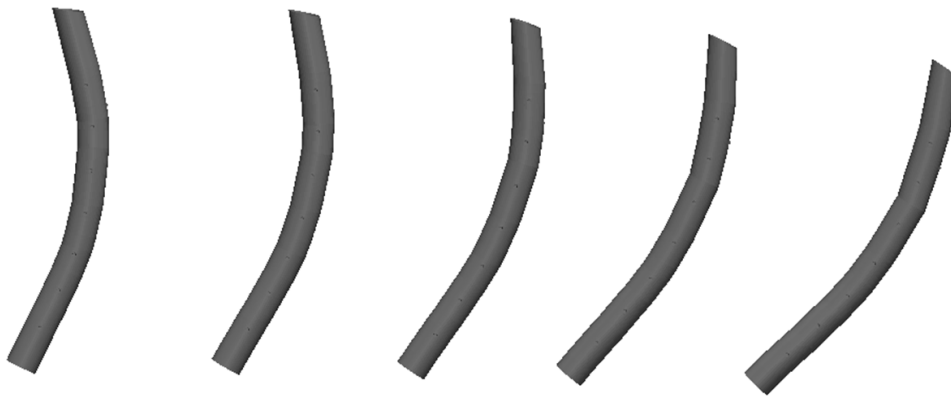


Figure 26 Position and shape of the model at $t = 0.19, 0.20, 0.21, 0.22$ and 0.23 s, respectively

3.2 FE simulations

From the FE simulations, the effect of crash pulses and various parameters on NIC and facet joint strains are discussed in the following section.

3.2.1 Neck Injury Criterion (NIC)

The Neck Injury Criterion (NIC) values for crashes involving the head restraint and crashes without head restraint are compared to assess the influence of the head restraint in reducing the neck injuries. Also an emphasis is made on the importance of the seating posture and the head restraint position on the neck injury outcome.

NIC is calculated by recording the accelerations at the centre of gravity of the head and the T1 vertebra in the THUMS model. The acceleration signals are filtered using CFC (Channel Frequency Class, digital filter) 180 and CFC 1000 respectively as per the standards of ISO/TC22/SC12/WG6 N 750. The NIC is intended to be calculated at maximum retraction (Boström *et al.*, 1996). Boström *et al.* (2000b) proposed the NIC_{max} which is the peak NIC value during first 150 ms. In this work, the analysis of

NIC is made during the first 150 ms of the simulation. However, the trend of NIC over the complete simulation is shown in Figures 27, 28 and 29. Since the critical limit for NIC is $15\text{m}^2/\text{s}^2$ (see Section 1.4), all the configurations are evaluated using this limit.

Comparing Figures 27 and 28, it is seen that NIC_{max} values in the presence of head restraint for the crash pulses of 2.5g and 5g are considerably lower compared to the corresponding values of NIC_{max} for cases without head restraint.

Observing Figure 27, the NIC value peaks at the time of head to head restraint contact for impacts with crash pulses 2.5g and 5g in the presence of head restraint. NIC_{max} for 5g occurs sooner in time compared to 2.5g pulse because the head to head restraint contact occurs earlier in the 5g crash pulse. However, the NIC_{max} for the 7.5g crash pulse occurs later than the 2.5g and 5g crash pulses because at severe crash pulses there is a high load acting on the seat. Hence the seat deflects backwards thus increasing the head to head restraint contact time. NIC_{max} values in the presence of head restraint for crash pulses of 2.5g and 5g are within the critical limit of $15\text{m}^2/\text{s}^2$ (refer Section 1.4) implying that the occupant is most likely free from suffering neck injury.

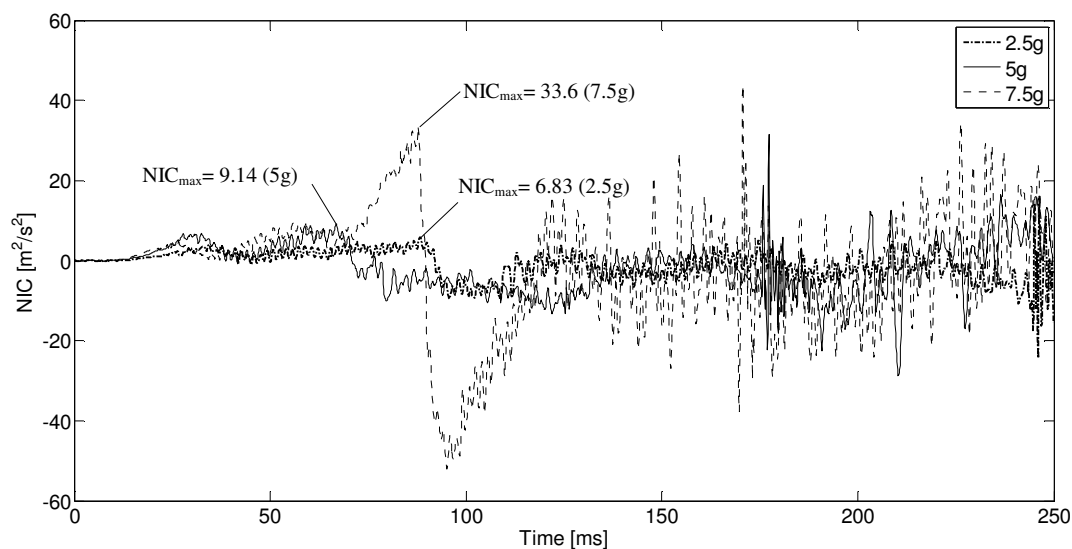


Figure 27 NIC values for various crash pulses with head restraint

For the cases without head restraint involving severe crash pulses of acceleration magnitudes 5g and 7.5g, the NIC_{max} is beyond the critical limit of $15\text{m}^2/\text{s}^2$. This implies that the occupant is at high risk of suffering from a severe long term neck injury. Also, NIC_{max} is observed before the head to head restraint contact, this suggests that the head restraint has no influence on reducing the injury severity in such a scenario.

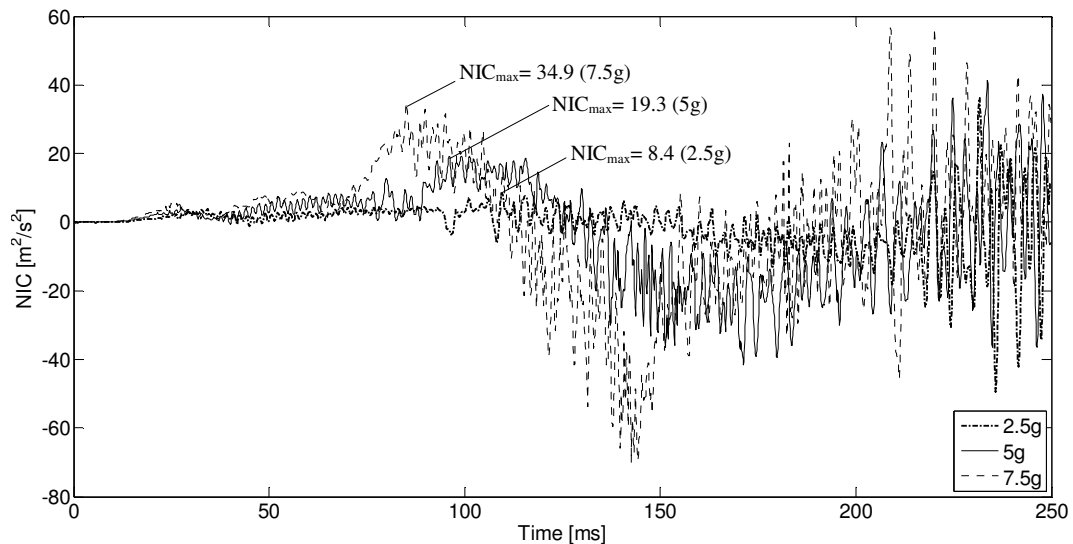


Figure 28 NIC values for various crash pulses without head restraint

3.2.2 Influence of Head Restraint Position and Occupant Posture

3.2.2.1 Influence of Head Restraint Position

As shown in the Table 2, an attempt is made to study the influence of the distance between head to head restraint and influence of seating posture on the severity of injury outcome.

To study the influence of the head restraint position a crash simulation with the crash pulse of 7.5g is performed with an increase in the distance between head to head restraint by 7 cm. The results obtained are compared to the configuration with the normal head restraint position for the same intensity of crash pulse, see Figure 29. It is observed that the NIC_{max} values for both cases are the same. This is because in both cases NIC peaks before the head to head restraint contact.

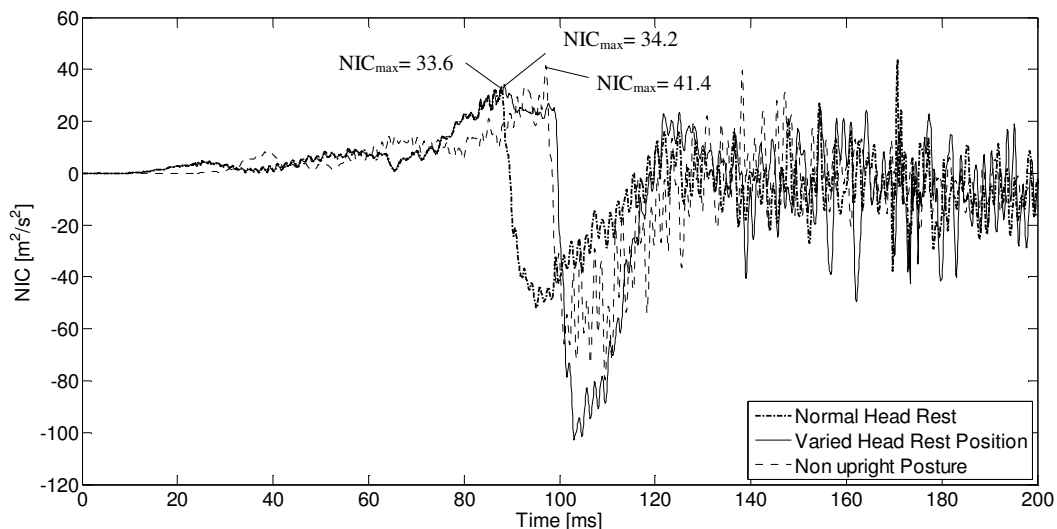


Figure 29 NIC for different head restraint position and seating posture

3.2.2.2 Influence of Seating Posture

During driving, at times the driver is not at his best seating position. To evaluate the effect of seating position on the outcome of injury severity a crash simulation is performed by seating the THUMS in a non-upright position as seen in Figure 30. The seating posture is such that pelvis is not in close contact with the back rest of the seat ('a' in Figure 30). Also, the back of the THUMS is not completely in contact with the back rest of the seat ('b' in Figure 30). Further, the head to head restraint distance is larger when seated in this non-upright posture ('c' in Figure 30). This position results in a larger curvature of the spine compared to the upright position.

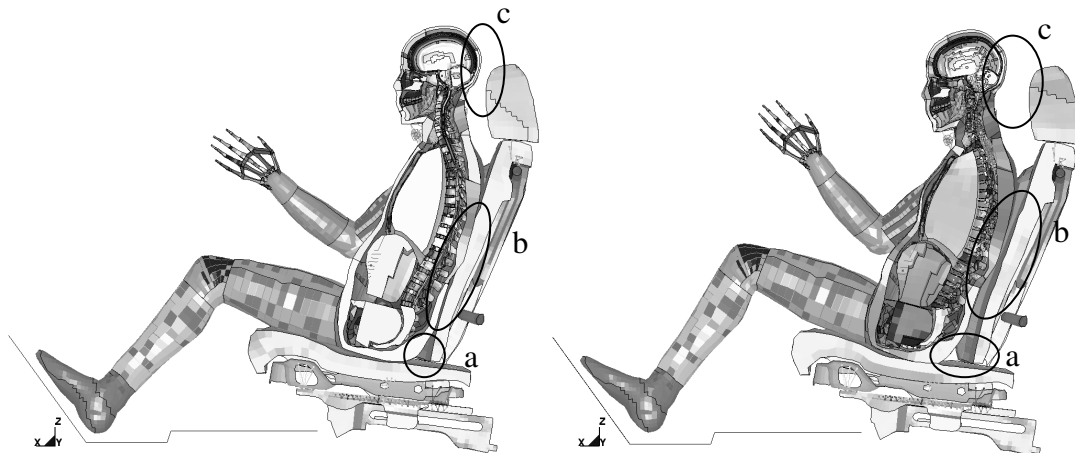


Figure 30 THUMS in upright (left) and non-upright posture (right)

Figure 29 shows that sitting in a non-upright position results in a higher NIC_{max} value compared to the NIC_{max} value attained when seated with upright posture. This is because there is a gap between the back of the driver to the seat back which results in higher acceleration of the T1 vertebra. In addition, the distance between the head to head restraint is higher which increases the head to head restraint contact time. All these factors contribute to higher NIC. This result emphasises the importance of the seating posture on the severity of neck injury outcome during crashes.

The severity of the injury can be reduced by moving the head restraint closer to the head of the driver. This results in quicker contact between the head and the head restraint which results in lower accelerations of the head and torso of the driver. This mitigates the injury outcome.

3.2.3 Facet Joint Strains

The facet joint capsule strain computations in this work are presented in *Table 5*.

Table 5 Facet joint capsule strain for various configurations. The value in bold suggests the capsule experiencing the maximum strain

Acceleration Pulses	Strains (With Head Restraint)					
	C2 - C3	C3 - C4	C4 - C5	C5 - C6	C6 - C7	C7 - T1
2.5g	0.0342	0.0368	0.1309	0.2062	0.1883	0.2151
5g	0.2265	0.2037	0.2759	0.2612	0.2076	0.2944
7.5g	0.2893	0.2633	0.3482	0.3290	0.2843	0.3763
Strains (Without Head Restraint)						
2.5g	0.1715	0.1712	0.4301	0.7561	0.5989	0.5792
5g	0.4814	0.3383	0.5117	0.9172	0.6456	0.5791
7.5g	0.4029	0.3088	0.5132	0.9236	0.6067	0.9326

Table 5 shows the strains experienced by facet joint capsule between each vertebra from C2 to T1 in the rear-end impacts with and without head restraint for 2.5g, 5g and 7.5g crash pulses. The values in bold suggests the capsule experiencing the maximum strain for a given crash condition. The influence of head restraint in lowering the strains in facet joint capsule is evident from Table 5. It is seen that for all the configurations, the same capsules experience more strain in the absence of head restraint. Also for impacts with head restraint, the facet joint capsule between C7 and T1 experiences the maximum strain. Similarly for the crashes without head restraint, the facet joint capsule between C5 and C6 experiences the maximum strain. However, for the case with 7.5g crash pulse, the strain in capsule between C7 and T1 experiences a slightly higher amount of strain.

The trend observed is the same for all the scenarios, hence only the cases involving crashes with accelerating pulse of 5g with and without head restraint are discussed in details. Here, the effect of head restraint on the facet joint strains is discussed. The trends for the remaining cases are shown in Appendix A.

The strains resulting in the facet joints during the crash simulations with an acceleration pulse of 5g both with and without head restraint are shown in Figures 31-36. Since large amount of strains are observed in the capsules between C5-C6, C6-C7 and C7-T1, only these vertebrae are considered for the analysis. An attempt is made to correlate these strains to the relative rotational and translational displacements of the C5, C6, C7 and T1 vertebrae.

Figures 31 and 32 show that there is a quite large difference in the magnitudes of strain in the facet joint capsules for the two cases with acceleration pulse of 5g. In both cases, the maximum capsule strain is seen between the C7 and T1 vertebrae. The difference in the magnitude is due to the different degree of relative rotational and translational displacement of the corresponding vertebrae.

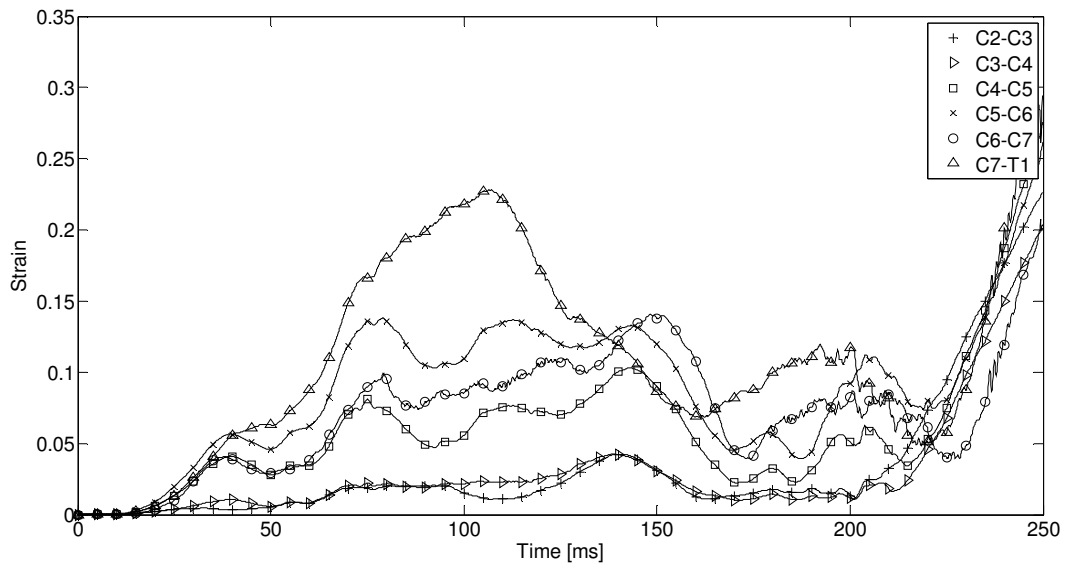


Figure 31 Facet joint capsule strains for crash pulse of 5g and with head restraint

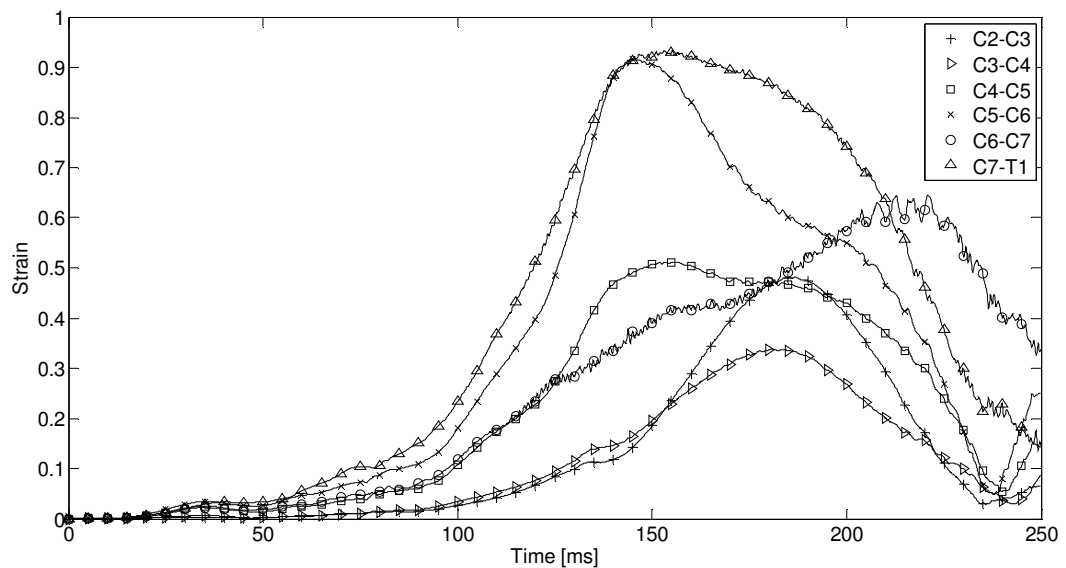


Figure 32 Facet joint capsule strains for crash pulse of 5g and without head restraint

Figures 33 and 34 show the relative anterior-posterior displacement of the vertebrae. It can be observed that the relative displacement between the vertebrae is considerably higher in the absence of a head restraint. This is because there is a larger extension of the neck when there is no head restraint, which results in a larger displacement of the vertebrae causing excessive shearing of the facet joint capsules.

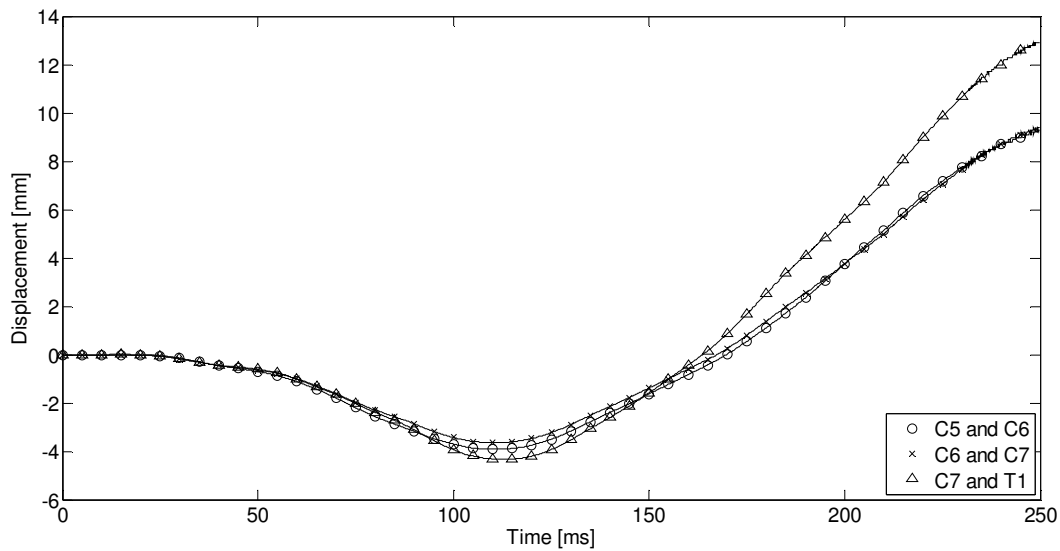


Figure 33 Relative anterior-posterior displacement of C5, C6, C7 and T1 vertebrae for a crash pulse of 5g and with head restraint

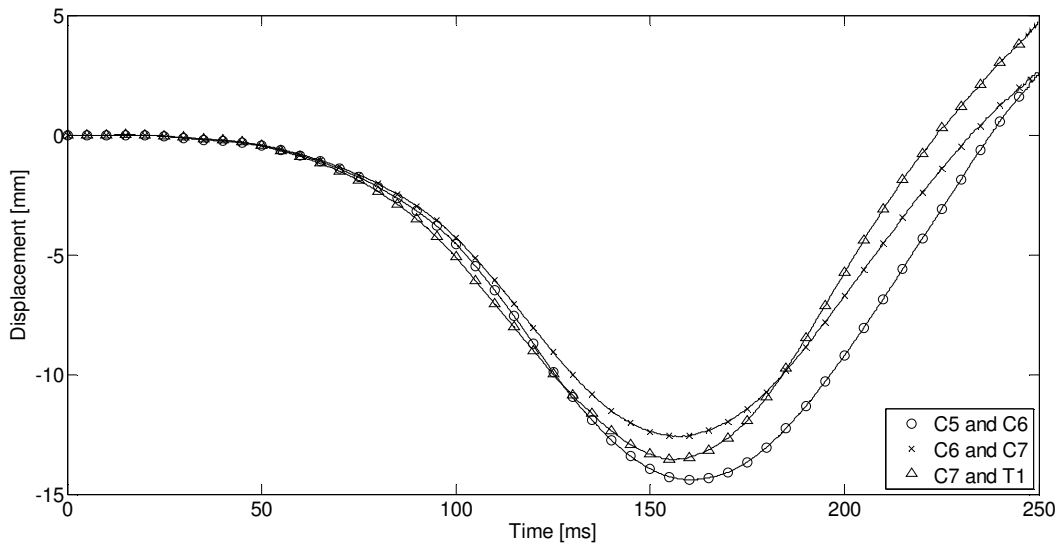


Figure 34 Relative anterior-posterior displacement of C5, C6, C7 and T1 vertebrae for a crash pulse of 5g and without head restraint

Shearing of the facet joint capsules takes place not only due to the translational displacement of the vertebrae but also due to the rotational displacement of the vertebrae. Figures 35 and 36 show the difference in the relative rotational displacement of the vertebrae for both cases. A high rotational displacement of the vertebrae is seen in the absence of the head restraint. This is also due to hyper-extension of the neck in the absence of a head restraint.

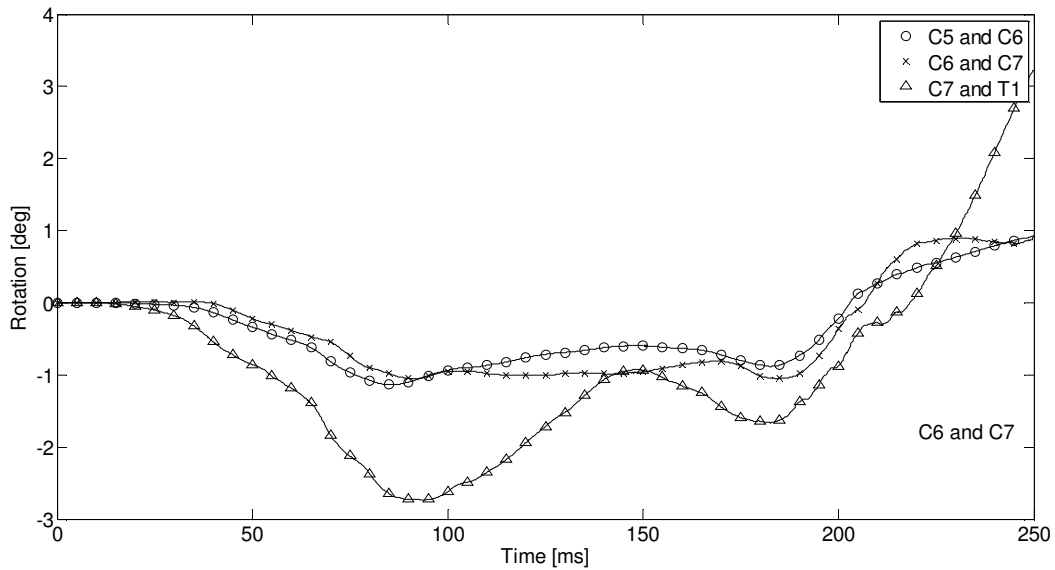


Figure 35 Relative rotational displacement of C5, C6, C7 and T1 vertebrae for a crash pulse of 5g and with head restraint

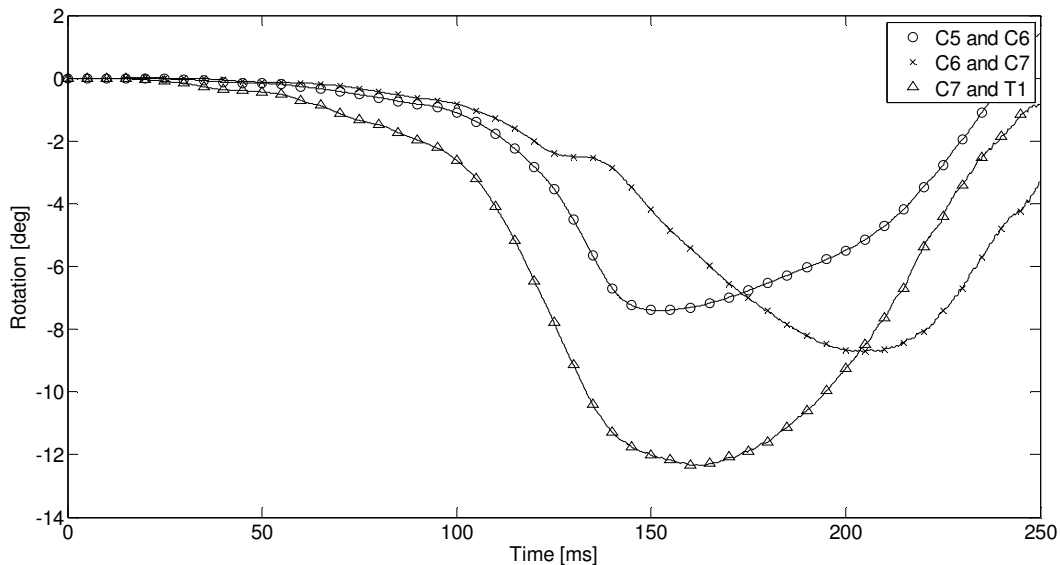


Figure 36 Relative rotational displacement of C5, C6, C7 and T1 vertebrae for a crash pulse of 5g and without head restraint

The facet joint capsule strain reaches its maximum value at maximum relative translational and rotational displacement, which takes place at around 160 ms when the maximum longitudinal velocity occurs (shown in Figure 21). This results in shearing of the facet joint capsule which in turn results in their deformation, as mentioned in Section 1.5.

The magnitude of the strain in the capsules is lower in the presence of the head restraint when compared to the configurations without head restraint. This implies that the head restraint has considerable influence on the facet joint capsule strains. This is because the presence of head restraint results in lower extension of the neck. This leads to smaller displacements of the vertebrae which result in smaller deformation of the capsules. This reduces the strain induced in the capsules.

3.3 CFD simulations

In this section, the discussion about the convergence of the fluid dynamics problem, the behaviour of the pressure through the network of blood vessels and the behaviour of the blood flow velocity are presented.

3.3.1 Convergence

As discussed in Section 2.4.5, initially the fluid dynamics problem is solved considering the blood as incompressible fluid and a solver based on the PISO algorithm is used. The solution achieved with these definitions is not converging and it can be checked by the pressure and velocity residuals in each time step. Hence, to achieve convergence at each time step SIMPLE algorithm is used.

In a transient problem, it is important that all time steps are fully converged. The number of iterations in the SIMPLE algorithm is, therefore, set to a high value. Figure 37 shows the number of iterations needed at each time step to reach a residual of 10^{-6} , which ensures the convergence. It is seen that in the first time steps the number of iterations needed is higher than afterwards. The residuals of pressure and velocity are always below this threshold, however, their value increase at about 0.1 s.

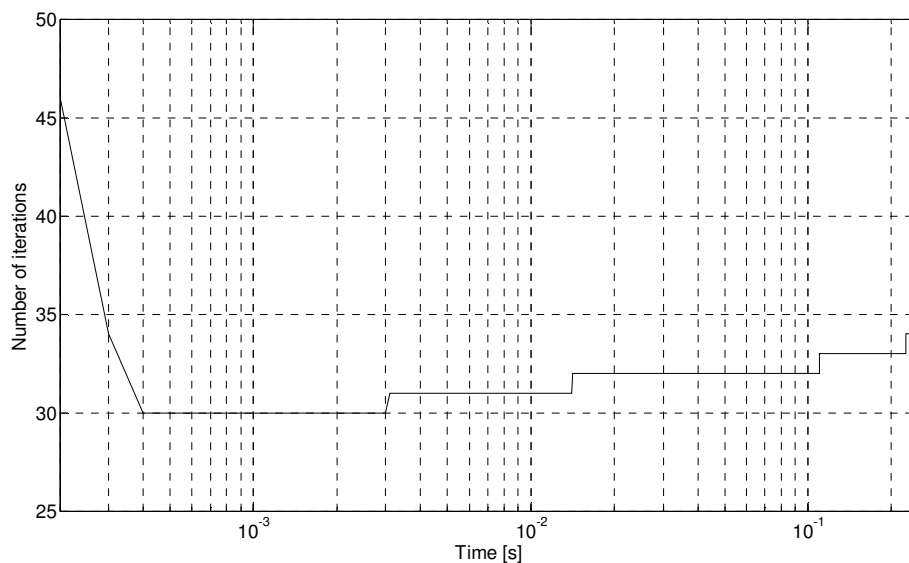


Figure 37 Number of iterations to reach convergence in each time step

3.3.2 Behaviour of the Pressure

Figure 38 shows a lot of fluctuations in the pressure when considering the blood to be incompressible for the configuration of 5g and with head restraint. These are four consecutive time steps and the negative and positive pressures exchange their position in each time step. The pressure values (p) shown are relative pressure divided by blood density, where the reference pressure value (p_{ref}) is the atmospheric pressure (10^5 Pa).

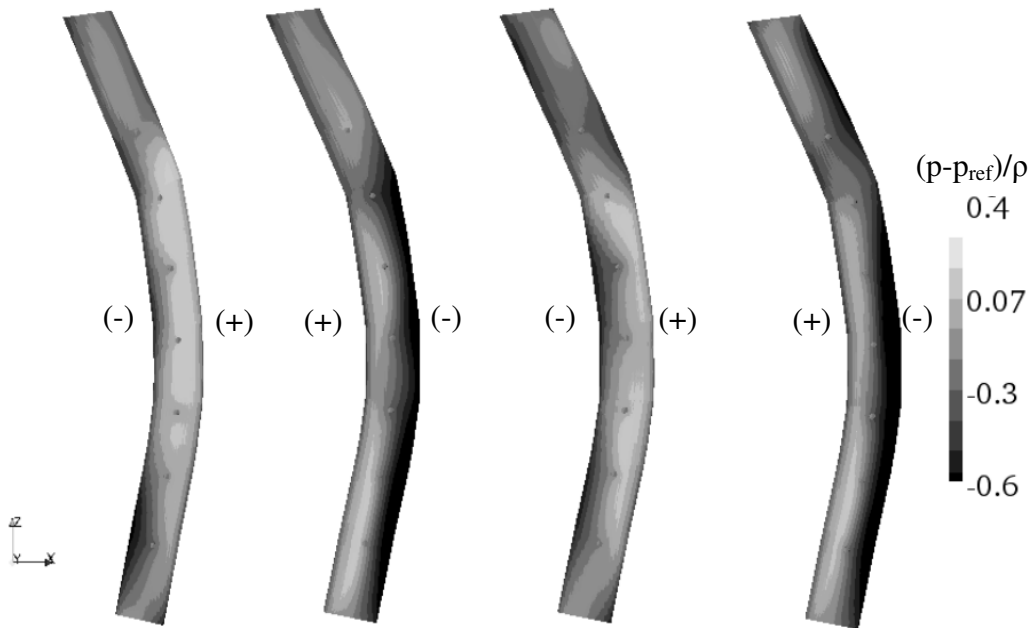


Figure 38 Fluctuating pressure distribution at $t = 0.07, 0.0701, 0.0702$ and 0.0703 s

The fluctuations mentioned just previously are also visible in time history of the pressure data. However, different trends of the pressure for the different rigid cylinders are visible by filtering their pressure data and averaging it for each rigid cylinder, see Figure 39. The filtering at a point is done by averaging 30 time steps on either sides of this point.

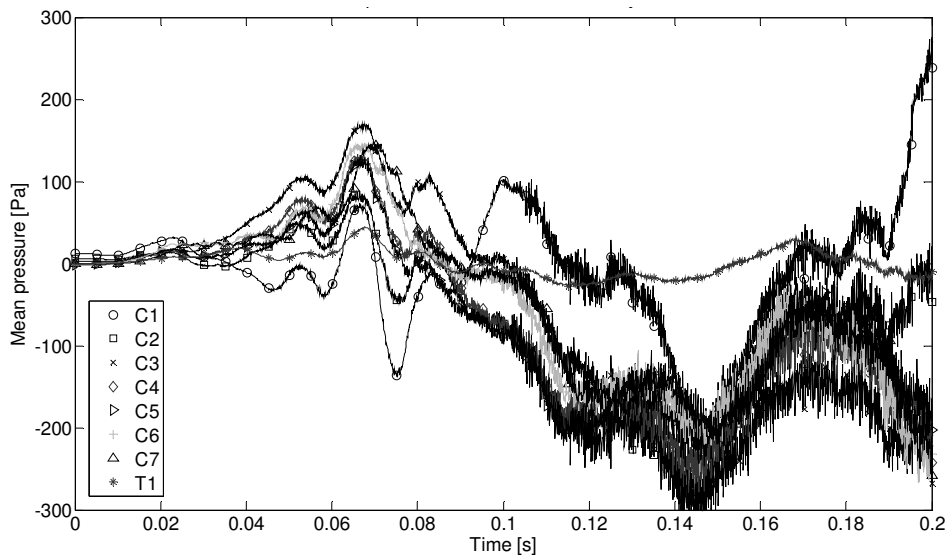


Figure 39 Mean pressure for the different rigid cylinders

Observing the trends of pressure in Figure 39, all the cylinders show some fluctuations just before reaching time 0.09 s. Afterwards a decrease in the pressure takes place and the signal becomes noisier. This increase of the noise in the signal corresponds to the increase of the pressure and velocity residuals mentioned in Section 3.3.

As it is mentioned, the pressure fluctuates even when converging. This could be due to either of the following reasons: infinite propagation of pressure waves in the incompressible formulation, resonances in the system and having extremely thin channels where the blood flows through.

Based on the study of Cedric (2008), the addition of compressibility seems to be the approach to avoid the fluctuations. The fact of adding compressibility into the definitions of the blood implies a change on the solver.

3.3.3 Behaviour of the Velocity

The blood flows through the venous plexus in several directions. The relative velocity (U_{rel}) of the flow is calculated by subtracting the velocities of the mesh motion from the absolute velocities calculated in the model. The relative velocity is averaged for each rigid cylinder at some representative time steps and is shown in Figure 40, Positive velocity is when the blood flows upwards and negative is when the blood is flowing downwards.

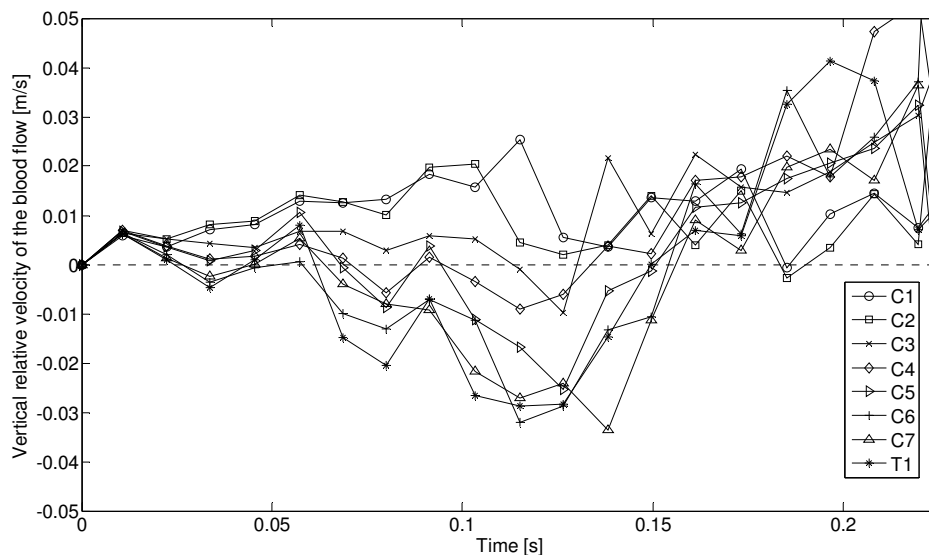


Figure 40 Vertical relative velocity of the blood flow for the different rigid cylinders

The blood flow in the cylinders representing the vertebrae C1 and C2 is going upwards as showing positive velocities in nearly all the time domain. The flow through C3 is mainly behaving in the same way as C1 and C2 except for an interval of time, from 0.1 s until 0.15 s. For this interval of time, the flow goes downwards and reaches its peak negative value at the same time in which the maximum extension takes place, at about 0.115 s. For the rest of the cylinders (C4, C5, C6, C7 and T1), the same kind of trend it is observed between them having nearly always higher velocities in T1 and lower velocities in C4. For these cylinders, from 0 s until 0.05 s the blood flow fluctuates going upwards and downwards. After 0.05 s, the flow continues going down with a slow down on the speed around 0.8 s and then speeding up down until reaching the peak speed in between 0.11 and 0.14 s (see Figure 41), around the point of maximum extension. Since then, the blood flow slows down and even changes the

direction to go up as the blood flow through the vertebrae C1, C2 and C3 does (see Figures 42 and 43); this change of direction takes place at around 0.155 s when the maximum longitudinal speed is achieved.

Figures 41, 42 and 43, show the relative speed by plotting arrows. The arrows show the direction of the relative velocity and their size is proportional to the velocity value. More figures with the blood behaviour through the model are added in Appendix B.

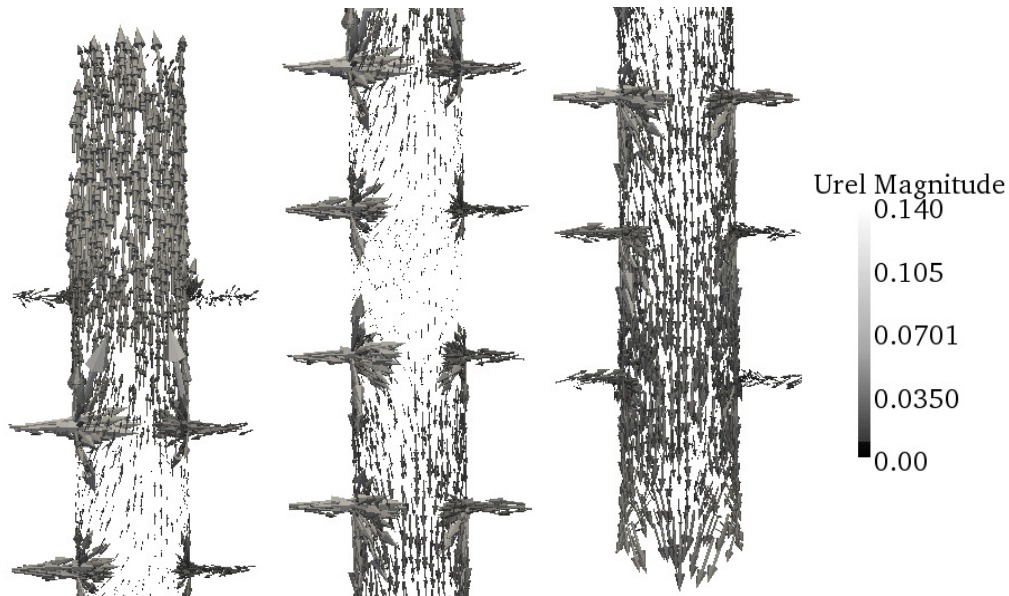


Figure 41 Blood flow through the entire model at 0.1209 s; top of the model (left), center (middle), bottom (right)

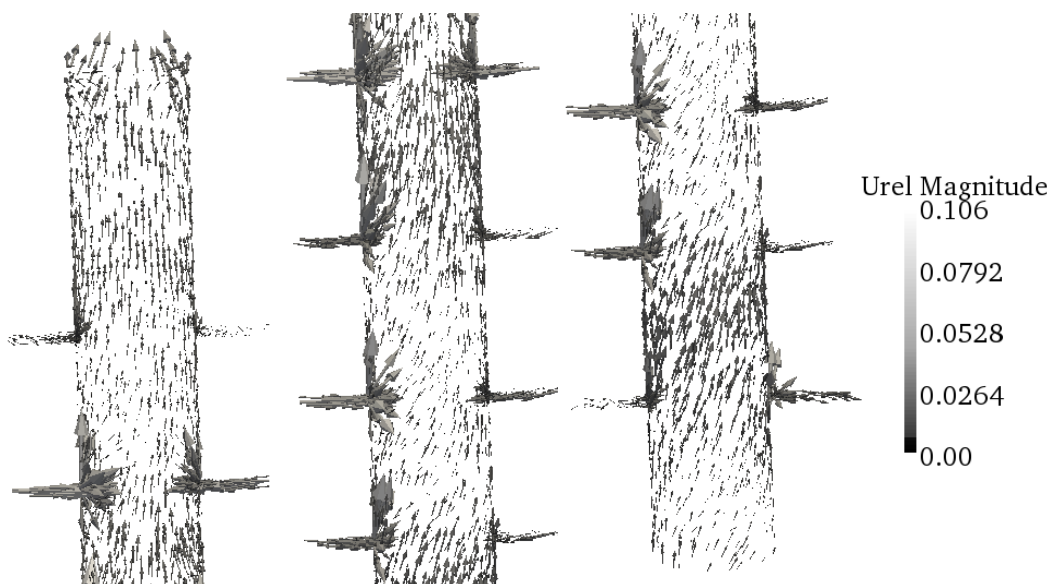


Figure 42 Blood flow through the entire model at 0.1761 s; top of the model (left), center (middle), bottom (right)

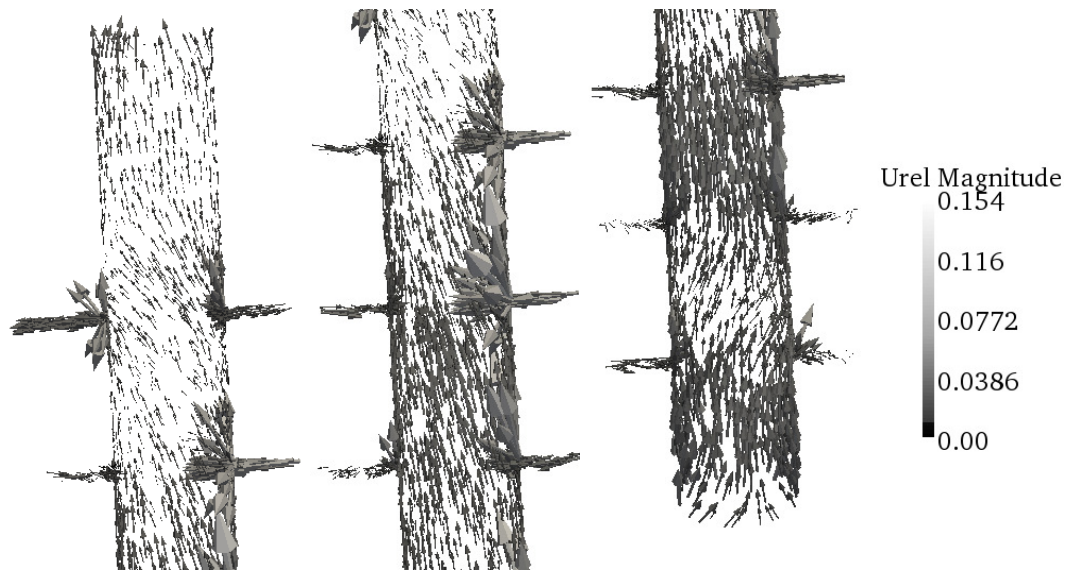


Figure 43 Blood flow through the entire model at 0.1897 s; top of the model (left), center (middle), bottom (right)

4 Conclusion

This work indicates the possibility of integrating FE modelling with CFD to gain better insights into injury site of the Whiplash Associated Disorders (WAD). In this work, THUMS model and driver seat model from Ford Taurus is used to simulate occupant to seat interaction in rear-end impacts. Neck Injury Criterion (NIC) and facet joint capsule strains are analyzed for different conditions and crash pulses of delta-V 15 km/h with magnitudes of 2.5g, 5g and 7.5g.

From this work, it is evident that head restraint plays a major role in reducing the injury severity in all crash scenarios. For the configurations with head restraint and crash pulses of 2.5g and 5g, the seat model from Ford Taurus is effective in limiting the value of NIC to $15 \text{ m}^2/\text{s}^2$. This indicates that occupant in this situation has low risk of suffering from WAD. However, for a severe crash pulse of 7.5g, the NIC value is $33.6 \text{ m}^2/\text{s}^2$ which indicates that the occupant has a high risk of long term neck injury. For the configurations with no head restraint, the NIC value is under the limit only for a crash pulse of 2.5g.

Facet joint capsule strain is considerably lower in the presence of head restraint compared to the corresponding strain values in the absence of head restraint. This is because the strain in the facet joint capsules is a function of relative anterior-posterior displacement along with the relative rotational displacement of the vertebrae. It is seen that the value of the strain peaks when the relative displacement between the vertebrae is maximum. Hence, it can be said that head restraint plays an important role in realizing lower joint capsule strains.

In addition, it can be concluded, that the solver to be used for the fluid dynamics problem should be based on SIMPLE algorithm. This algorithm solves the pressure-velocity equations by using the coupled iterations.

5 Future Scope

In this study an attempt is made to understand the relationship between pressure transients in the network of blood vessels and the injury severity along with the effect of various crash pulses and seating parameters on the injury risk. However, a further in-depth study would lead to better understanding of the injuries.

The steps that could be carried out to better understand the injuries are:

FE modelling:

- More number of possible configurations considering different seating postures, the positions of the head restraints, seat back stiffness and active head restraints should be evaluated. The effect of crash pulses with different acceleration peaks and delta-V should be analysed.
- Physiological factors for male and female occupants should be addressed.
- Analysis of N_{km} which is a neck injury criterion based on moments and forces acting in occipital joint. This will lead to a better understanding of neck injury.

CFD modelling:

- Consider the compressibility of the blood and the flexibility of the veins by using a SIMPLE-based solver.
- Run simulations with a geometry without a hole to avoid thin walls and the big ratio h (characteristic distance, see Section 2.4.4) to diameter of the side pipes.
- Incorporate the loss coefficient in the inlets and outlets to consider the flow resistance when exiting from the model.
- Consider the deformation of the model in radial direction to have a more realistic behaviour. Therefore, the inner volume change takes place in both radial and axial directions during extension and flexion of the neck.

6 References

6.1 Publications

- Boström, O., Svensson, M.Y., Aldman, B., Hansson H.A., Håland Y., Lövsund, P., Seeman, T., Suneson, A., Sälsjö, A., Örtengren, T. (1996) A New Neck Injury Criterion Candidate - Based on Injury Findings in the Cervical Spinal Ganglia after Experimental Neck Extension Trauma, *Proc. IRCOBI Conf.*, Dublin, Ireland, pp. 123-136.
- Brault, J.R., Wheeler, J.B., Siegmund, G.P., Brault, E.J. (1998) Clinical Response of Human Subjects to Rear-End Automobile Collisions, *Arch Phys Med Rehabil.* Vol. 79(1), pp. 72-80.
- Breig, A. (1978) Adverse Mechanical Tension in the Central Nervous System. Almquist & Wiksell Int., Stockholm, Sweden, ISBN 91-2200126-3.
- Cappon, H.J., Philippens, M.M.G.M., van Ratingen, M.R., Wismans, J.S.H.M. (2000) Evaluation of dummy behavior during low severity rear impact, *Proc. IRCOBI Conf.*, Montpellier, France.
- Cappon H, Philippens M, Wilmans J (2001) A new test method for the assessment of neck injuries in rear-end collisions. *Proc. 17th ESV Conference 2001*. Paper no 242.
- Cedric, G. (2008) *Modelling Whiplash Injuries using compressible CFD*, Master Thesis, Department of Applied Mechanics, Chalmers University of Technology, Göteborg, Sweden.
- Clemens, H.B. (1961) *The Migration, Age, and Growth of Pacific Albacore (Thunnus germo)*, 1951-1958. State of California, Department of Fish and Game, Fish Bulletin 115, pp 128.
- Deng, B., Begeman, P.C., Yang, K.H., Tashman, S., King, A.I. (2000a) Kinematics of Human Post mortem human subject Cervical Spine During Low Speed Rear-End Impacts, *Proc. 44th Stapp Car Conf. Journal*, Paper No. 2000-01-SC13, pp. 171-188.
- EASI Engineering (2007) Whiplash Test- Bewertungsverfahren beim Heckaufprall. Kompaktseminar EASI Trainingscenter Alzenau, February 2007.
- Eriksson, L. (2004) *Neck injury risk in rear-end impacts-Risk factors and neck injury criterion evaluation with Madymo modelling and real life data*, degree of doctor of philosophy thesis, Chalmers University of Technology, Göteborg, Sweden, pp. 78
- Estes, M.S., McEkhaney, J.H. (1971) Response of Brain Tissue of Compressive Loading. *Proceedings of the 4th ASME J. Biomechanics Conference*, Paper no. 70-BHF-13.

- Galasko, C. S. B. (1996). Whiplash associated disorders: Cost to society, *Proc. Whiplash '96*, p. 55.
- Håland, Y., Lindh, F., Fredriksson, R., Svensson, M.Y. (1996) The Influence of the Car Body and the Seat on the Loading of the Front Seat Occupant's Neck in Low Speed Rear Impacts, *29th ISATA*, Florence, Italy.
- Hell, W., Langwieder, K., Walz, F., Muser, M., Kramer, M., Hartwig, E. (1999) Consequences for seat design due to rear end accident analysis, sled tests and possible test criteria for reducing cervical spine injuries after rear-end collisions, *Proc. IRCOBI Conf.*, Sitges, Spain, pp. 243-259.
- Hofinger M., Mayrhofer E., Geigl B., Moser A., Steffan H. (1999) Reduction of Neck Injuries by Improving the Occupant Interaction with the Seat Back Cushion, *Proc. IRCOBI Conf.*, Sitges, Spain.
- Jakobsson, L., Norin, H. (1999) Suggestions for evaluation criteria of neck injury protection in rear end car impacts, *Proc. IRCOBI Conf.*, Barcelona, Spain, pp. 271-282.
- Jakobsson, L., (2000) *AIS 1 neck injuries in rear-end car impacts*, Licentiate Thesis, Department of Machine and Vehicle Design, Chalmers University of Technology, Göteborg, Sweden.
- Jakobsson, L., Lundell, B., Norin, H., Isaksson-Hellman, I. (2000) WHIPS - Volvo's Whiplash Protection Study. *Accident Analysis & Prevention*, Vol. 32(2), pp. 307-319.
- Kapandji, I.A. (1974) *The Physiology of the Joints, Volume Three*, Churchill Livingstone, Edinburgh, ISBN 0 443 01209 1.
- Krafft, M. (1998) *Non-fatal injuries to car occupants – Injury assessment and analysis of impact causing short- and long-term consequences with special reference to neck injuries*, Ph.D. Thesis, Karolinska Institute, Stockholm, ISBN 91-628-3196-8.
- Krafft M., Kullgren A., Lie A., Tingvall C. (2004) *Assessment of Whiplash Protection in Rear Impacts - Crash Tests and Real-life Crashes*. Stockholm, Sweden.
- Kitagawa, Y., Yasuki, T., Hasegawa J., (2006) A Study of Cervical Spine Kinematics and Joint Capsule Strain in Rear Impacts Using a Human FE Model. *Stapp Car Crash Journal*, Vol. 50, pp 545-566.
- Kullgren, A., Thomson, R., Krafft, M. (1999) The Effect of Crash Pulse Shape on AIS1 Neck Injuries in Frontal Impacts, *Proc. IRCOBI Conf.*, Sitges, Spain, pp. 231-242.
- Liu, F., Yang, J. (2008) *Modelling of Whiplash Injuries using CFD*, Master Thesis, Department of Applied Mechanics, Chalmers University of Technology, Göteborg, Sweden.

- Mertz, H.J., Patrick, L.M. (1971) Strength and Response of the Human Neck. *Proc. 15th Stapp Car Crash Conf.*, SAE Inc., New York, LC 67-22372, pp. 207-255.
- Molino L. (1998) Determination of Moment-Deflection Characteristics of Automobile Seat Backs, Light Duty Division, Office of Crashworthiness Standards, National Highway Traffic Safety Administration, USA, <http://www.nhtsa.dot.gov/cars/rules/CrashWorthy/Seats/deflrep1/deflrep1.html>
- Morishita, Y., Naito, M., Hymanson, H., Miyazaki, M., Wu, G., Wang, J.C. (2009) The Relationship between the Cervical Spinal Canal Diameter and the Pathological Changes in the Cervical Spine. *European Spine Journal*, Vol. 18 pp 877-883.
- Morris, A.P., Thomas, P. (1996) A Study of Soft Tissue Neck Injuries in the UK, *Proc. 15th ESV Conf.*, Melbourne, Australia, Paper No. 96-S9-O-08.
- Mukhin, S.I., Sosnin, N.V., Favorskii, A.P. (2006) The Effect of Viscous Friction on Pulse Waves. *Differentsial'nye Uravneniya*, Vol. 42, No. 7, pp. 979-993.
- NHTSA (1996) Head Restraints – Identifications of Issues Relevant to Regulation, Design and Effectiveness
- Nygren, Å. (1984) Injuries to car occupants - some aspects of the interior safety of cars. A study of a five-years material from an insurance company, *Akta Oto-Laryngologica*, Supplement 395, Almqvist & Wiksell, Stockholm, Sweden, ISSN 0365-5237.
- Ono, K., Kaneoka, K., Wittek, A., Kajzer, K. (2000) Cervical Injury Mechanism Based on the Analysis of Human Cervical Vertebral Motion and Head-Neck-Torso Kinematics During Low Speed Rear Impacts, *Frontiers in Whiplash Trauma*, vol. 38, p372-p388.
- Parkin S., Mackay G.M., Hassan A.M., Graham R. (1995) Rear End Collisions and Seat Performance - To Yield or Not To Yield, *Proc. 39th Annual AAAM Conf.*, Chicago, Illinois, pp. 231-244.
- Pike, J.A. (2000) Whiplash Injury and Vehicle Design Concepts, *Frontiers in Whiplash Trauma: Clinical & Biomechanical*, Yoganandan, N. and Pintar, F.A. (Eds.), ISO Press, Amsterdam, The Netherlands, ISBN 1 58603 912 4, pp. 41-44.
- Prasad, P., Kim, A., Weerappuli, D.P.V. (1997) Biofidelic Anthropomorphic Test Devices for Rear Impact, *Proc. 41st STAPP Car Crash Conf.*, SAE Paper No. 973342, USA, pp. 387-412.
- Ray. G. (2000) Mechanics of Low-Speed Impact and Implication in Injury Biomechanics, *Frontiers in Whiplash Trauma: Clinical & Biomechanical*, Yoganandan, N. and Pintar, F.A. (Eds.), ISO Press, Amsterdam, The Netherlands, ISBN 1 58603 912 4, pp.10-24.

- Schmitt, K.-U., Muser, M.H., Niederer, P. (2001) A neck injury criterion candidate for rear-end collisions taking into account shear forces and bending moment, *Proc. 17th ESV Conf.*, Amsterdam, The Netherlands, Paper No. 124.
- Sekizuka M. (1998) Seat Designs For Whiplash Injury Lessening, *Proc. 16th ESV Conf.*, Windsor, Canada, Paper No. 98-S7-O-06.
- Siegmund, G.P., King, D.J., Lawrence, J.M., Wheeler, J.B., Brault, J.R., Smith, T.A. (1997) Head/Neck Kinematic Response of Human Subjects in Low-Speed
- Stother C., James M. (1987) Evaluation of Seat Back Strength and Seat Belt Effectiveness in Rear End Impacts, SAE 872214, *Proc. 31st Stapp Car Crash Conf.*, New Orleans, LA, USA.
- Svensson, M.Y. (1993) *Neck-Injuries in Rear-End Car Collisions – Sites and biomechanical causes of the injuries, test methods and prevention measures*, Ph.D. Thesis, Chalmers University of Technology, Göteborg, Sweden, ISBN 91-7032-878-1.
- Svensson, M.Y., Aldman, B. Hanson, H.A., Lövsund, P., Seeman, T., Suneson, A., Örtengren, T. (1993) Pressure Effects in the Spinal Canal during Whiplash Extension Motion, *Proc. IRCOBI Conf.*, Eindhoven, The Netherlands, pp. 189-200.
- Svensson, M.Y., Boström, O., Davidsson, J., Hansson, H.A., Håland, Y., Lövsund, P., Suneson, A., Säljö, A. (1993) Neck injuries in car collisions – A review covering a possible injury mechanism and the development of a new rear-impact dummy, *Accident Analysis & Prevention*, Vol. 32, pp. 167-175.
- Thomson, R.W., Romilly, D.P., Narvin, F.D.P. Macnabb, M.J. (1993) Dynamic Requirements of Automotive Seatbacks, *International Congress and Exposition*, SAE Paper No. 930349, SP-963, Society of Automotive Engineers, Warrendale, PA.
- Tencer, A.F., Miraz, S., Martin, D., Goodwin, V., Sackett, R., Schaefer, J. (2000) Development of a Retro-Fit Anti-Whiplash Seat Cushion Based on Studies of Crash Victims and Human Volunteers, *Frontiers in Whiplash Trauma: Clinical & Biomechanical*, Yoganandan, N. and Pintar, F.A. (Eds.), ISO Press, Amsterdam, The Netherlands, ISBN 1 58603 912 4, pp. 491-509.
- Yoganandan, N., Pintar, F.A., Cusick, J.F., Kleinberger, M. (1998) Head-Neck Biomechanics in Simulated Rear Impacts, *Proc. 42nd Annual AAAM Conf.*, Charlottesville, VA, USA, pp. 206-231.
- Versteeg, H.K., Malalasekera, W. (2007) *An Introduction to Computational Fluid Dynamics – The Finite Volume Method*. Second Edition. Harlow (England): Pearson Education Limited.
- Whiplashkommissionen (Swedish Whiplash Commission) (2006) *Diagnosis and early management of Whiplash injuries*. Stockholm, Sweden.

- Winkelstein, B., Nightingale, R., Richardson, W., Myers, B. (1999) Cervical Facet Joint Mechanics: Its Application to Whiplash Injury. *Proc. 43rd Stapp Car Crash Conference*, San Diego, USA, pp 243-265.
- Wiklund, K., Larsson, H. (1998) SAAB Active Head Restraint (SAHR)- Seat Design to Reduce the Risk of Neck Injuries in Rear Impacts, *SAE International Congress and Exposition*, Detroit, MI, SAE Paper No. 980297. Warrendale, PA, Society of Automotive Engineers.
- Yang, K.H., Begeman, P.C. (1996) A Proposed Role for Facet Joints in the Neck Pain in Low to Moderate Speed Rear End Impacts, Part 1: Biomechanics, *6th Injury Prevention Through Biomechanics Symposium*, pp. 59-63.
- Yoganandan, N., Pintar, F.A., Cusick, J.F., Kleinberger, M. (1998) Head-Neck Biomechanics in Simulated Rear Impacts, *Proc. 42nd Annual AAAM Conf.*, Charlottesville, VA, USA, pp. 206-231.
- Zuby, D.S., Troy Vann, D., Lund, A.K., Morris, C.R. (1999) Crash Test Evaluation of Whiplash Injury Risk, *Proc. 43rd Stapp Car Crash Conf.*, San Diego, USA, Paper No. 99SC17, pp. 267-278.

6.2 Internet References

- Hughston Health Alert, 1997 [retrieved 2010-04-27].
 Accessible at: <http://www.hughston.com/hha/a.cspine.htm>
- Image-Guided Musculoskeletal Procedures, [retrieved 2010-04-27].
 Accessible at: http://members.cox.net/injections/selective_principles.htm
- OpenFOAMWiki, 2009 [retrieved 2010-05-11].
 Accessible at: <http://openfoamwiki.net>
- UHN Orthopaedics (Toronto Western Hospital), [retrieved 2010-04-27].
 Accessible at: www.eorthopod.com

Appendix A

Facet Joint Capsule Strains for 2.5 and 7.5g with and without Head Restraint

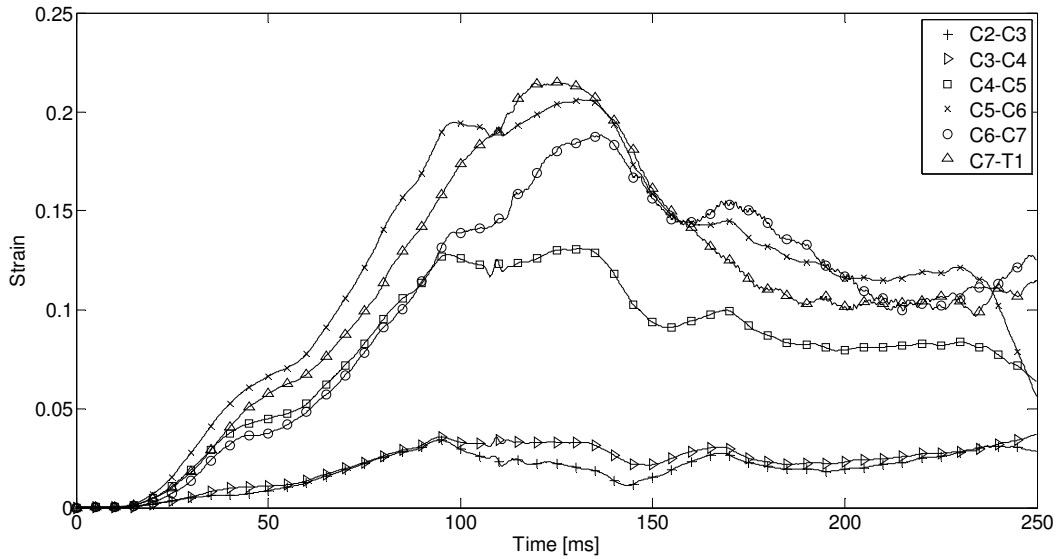


Figure 44 Facet joint capsule strain for 2.5g crash pulse with head restraint

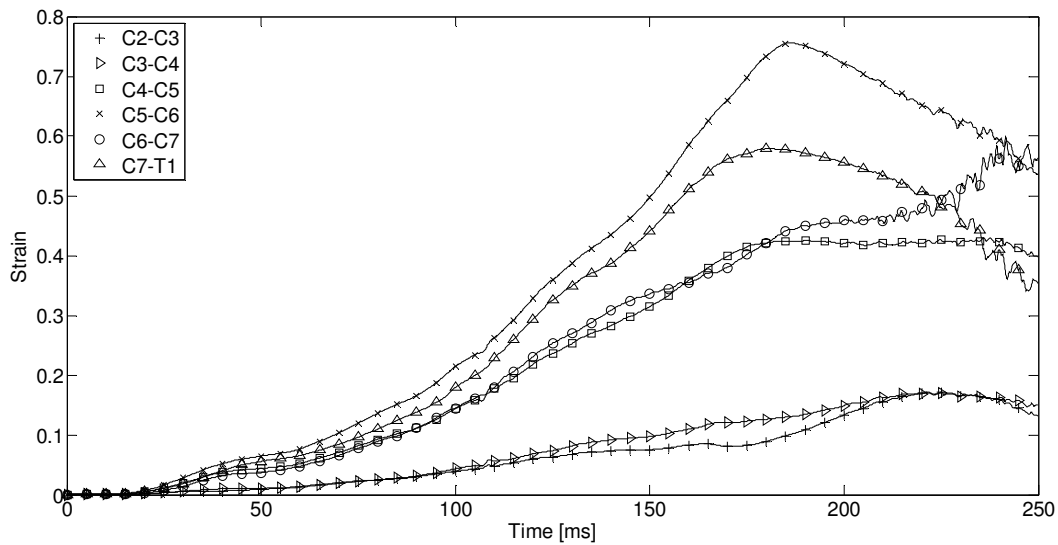


Figure 45 Facet joint capsule strain for 2.5g crash pulse without head restraint

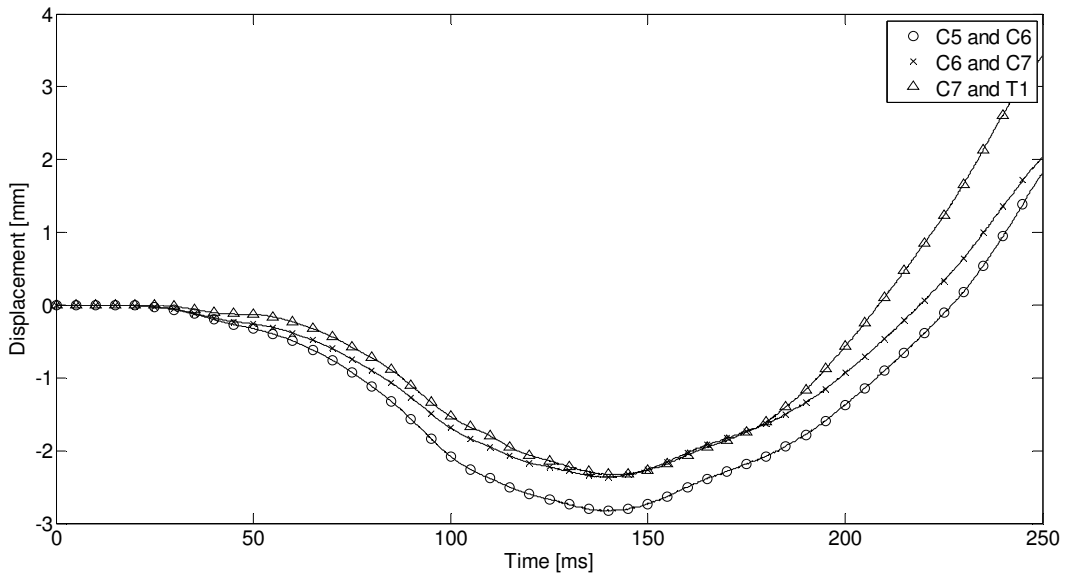


Figure 46 Relative anterior-posterior displacement of C5, C6, C7 and T1 vertebrae for a crash pulse of 2.5g and with head restraint

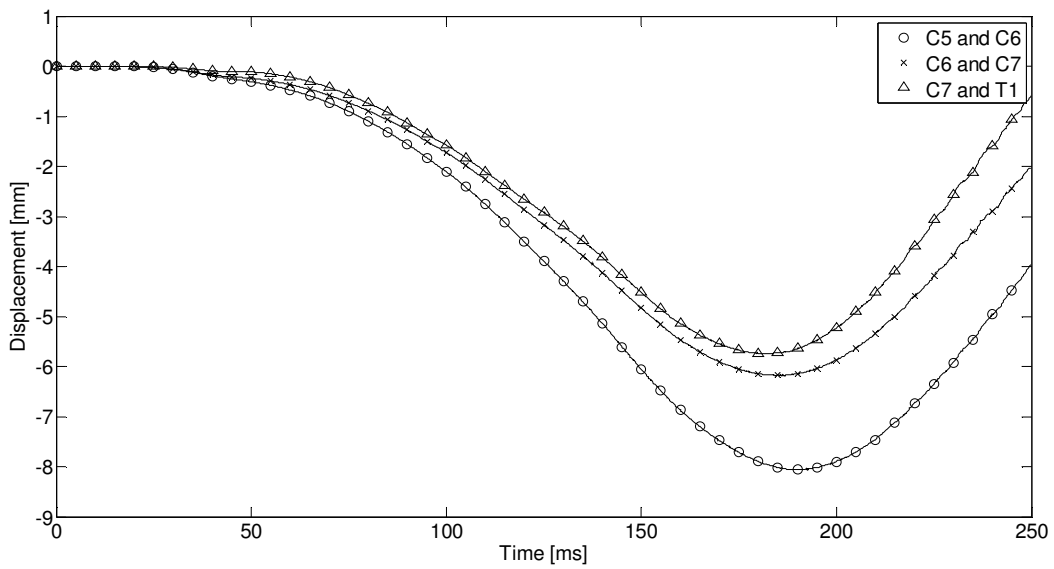


Figure 47 Relative anterior-posterior displacement of C5, C6, C7 and T1 vertebrae for a crash pulse of 2.5g and without head restraint

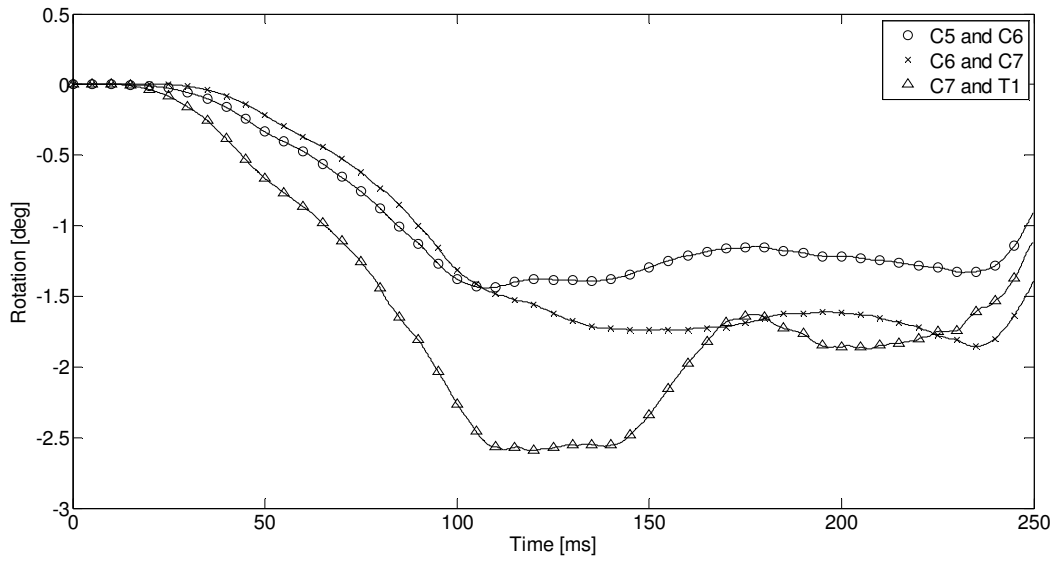


Figure 48 Relative rotational displacement of C5, C6, C7 and T1 vertebrae for a crash pulse of 2.5g and with head restraint

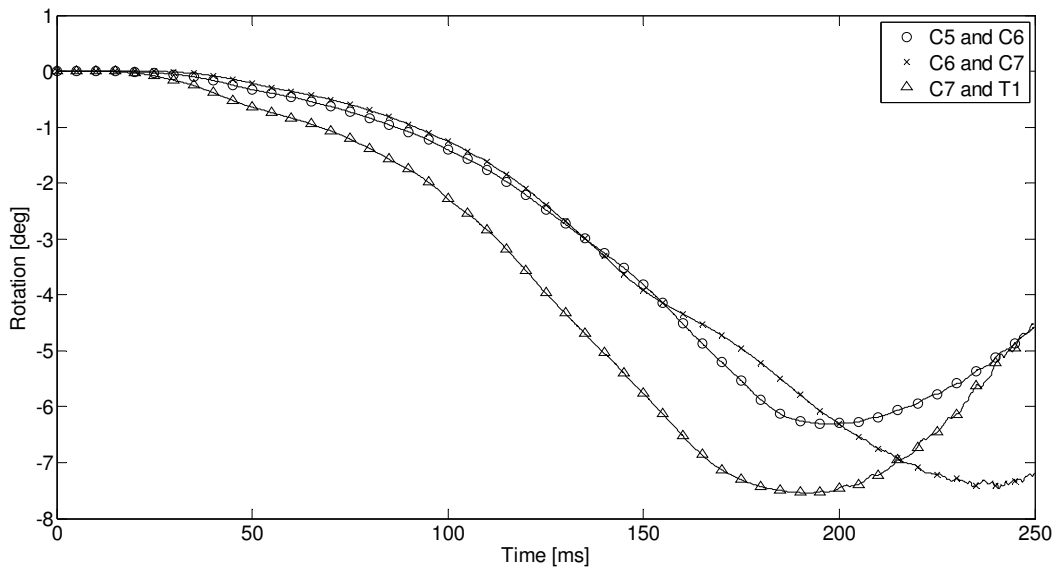


Figure 49 Relative rotational displacement of C5, C6, C7 and T1 vertebrae for a crash pulse of 2.5g and without head restraint

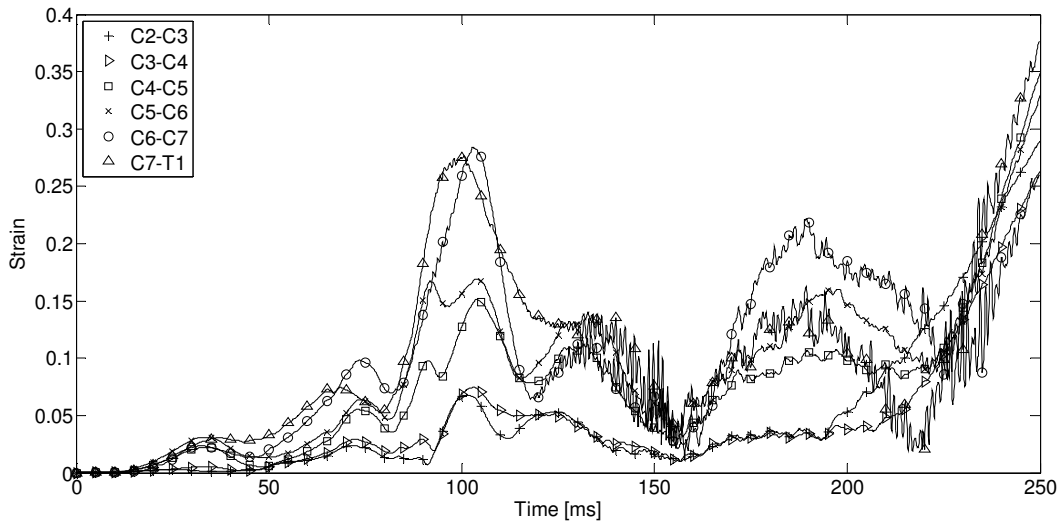


Figure 50 Facet joint capsule strain for 7.5g crash pulse with head restraint

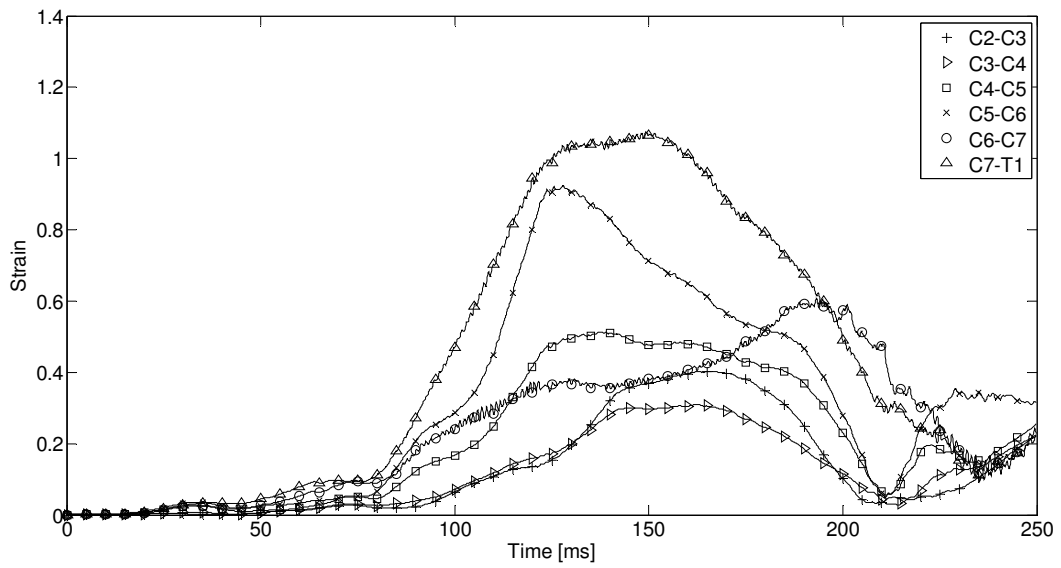


Figure 51 Facet joint capsule strain for 7.5g crash pulse without head restraint

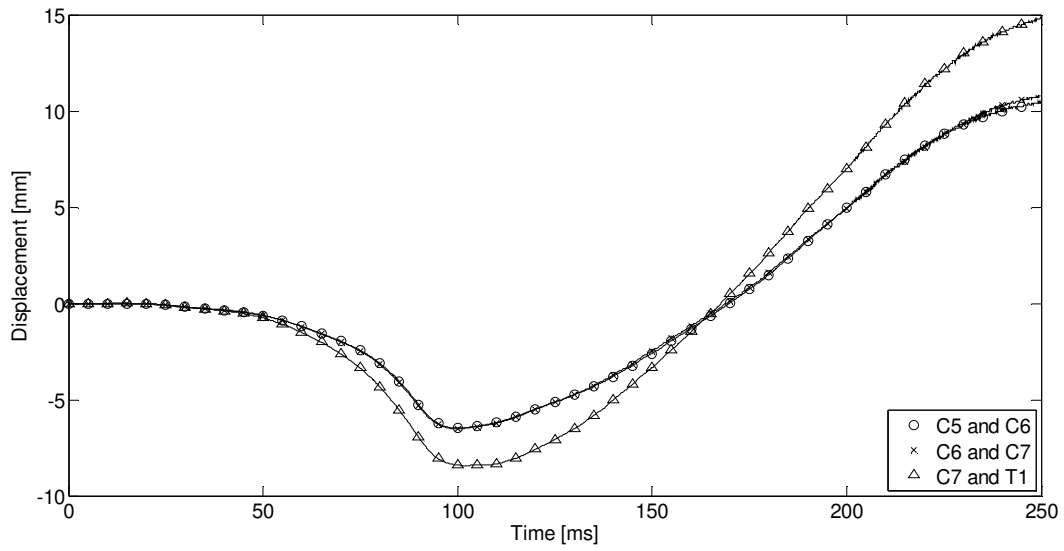


Figure 52 Relative anterior-posterior displacement of C5, C6, C7 and T1 vertebrae for a crash pulse of 7.5g and with head restraint

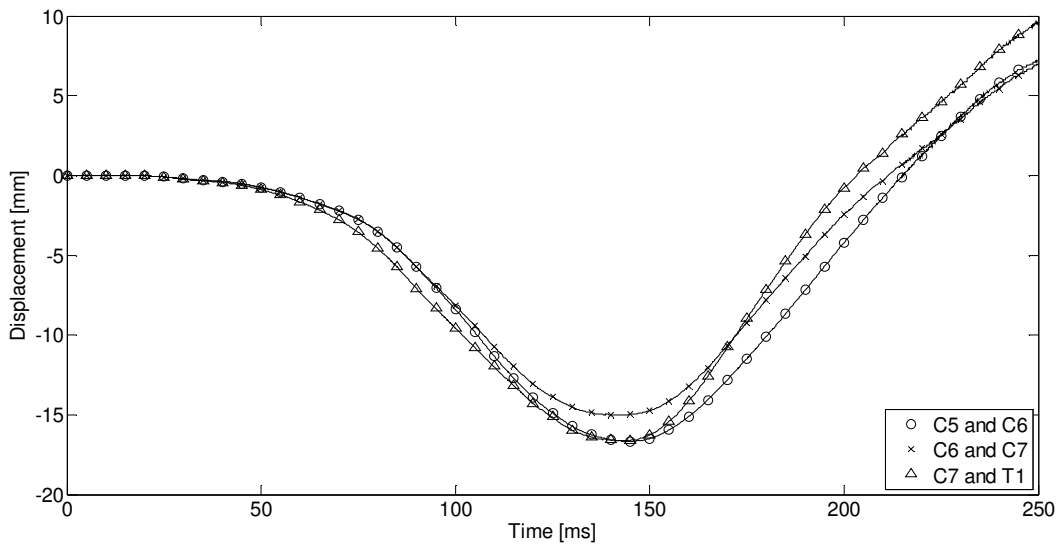


Figure 53 Relative anterior-posterior displacement of C5, C6, C7 and T1 vertebrae for a crash pulse of 7.5g and without head restraint

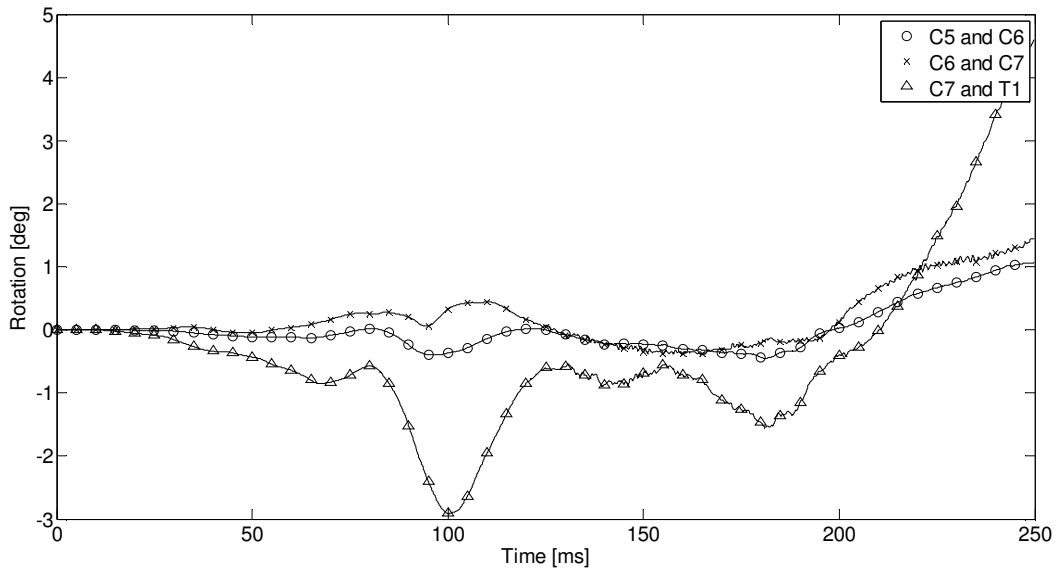


Figure 54 Relative rotational displacement of C5, C6, C7 and T1 vertebrae for a crash pulse of 7.5g and with head restraint

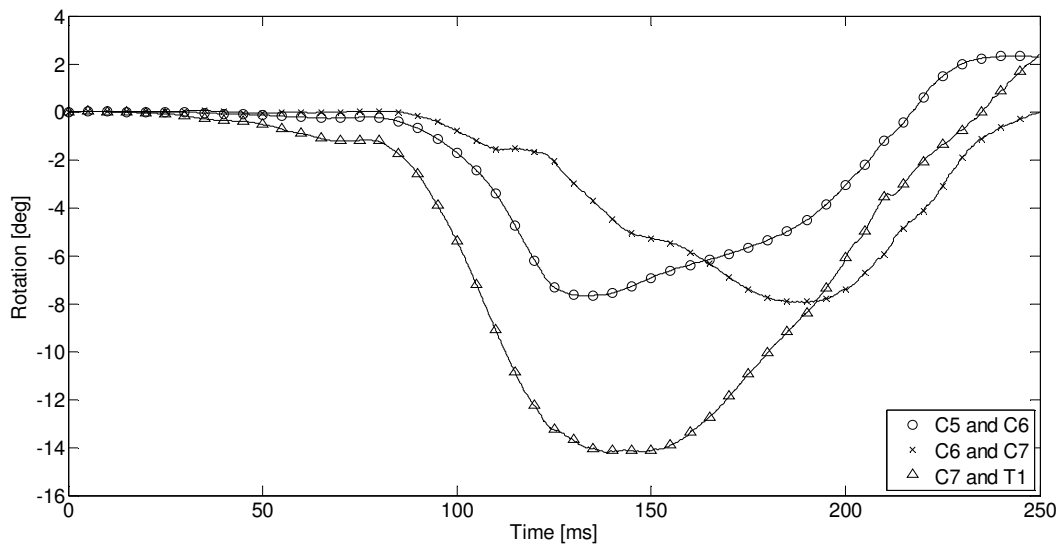


Figure 55 Relative rotational displacement of C5, C6, C7 and T1 vertebrae for a crash pulse of 7.5g and without head restraint

Appendix B

Blood Flow Through the Model

This appendix incorporate figures of the blood flow behaviour for the simulation with 5g acceleration pulse and head restraint. These figures are taken from Paraview, which is an open source scientific visualization. The relative velocity (U_{rel}) of the blood through the pipes representing the network of blood vessels is shown and it is represented by arrows, which show the direction of the flow and their size depends on the relative velocity value.

At the beginning of the simulation, the THUMS sinks into the seat and therefore the model goes downwards which results in an upwards relative velocity of the flow, see Figure 56.

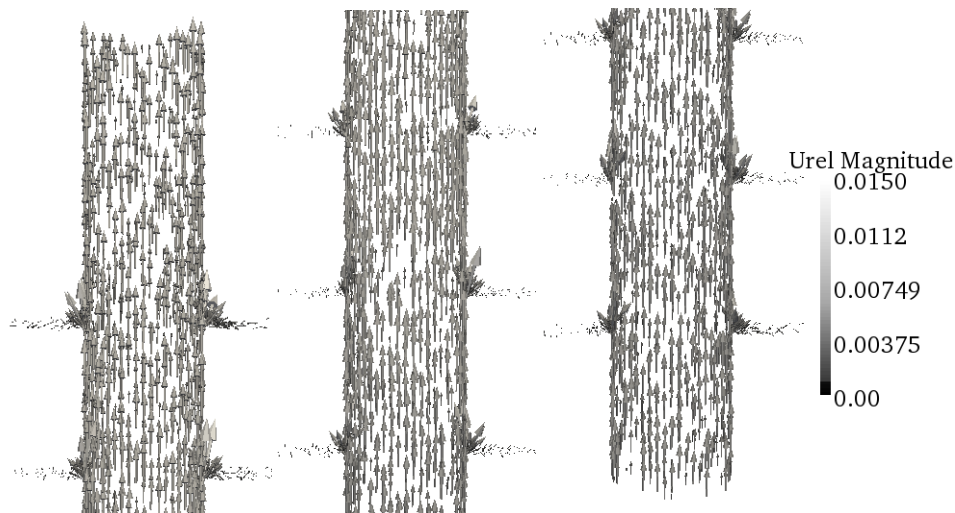


Figure 56 Blood flow through the entire model at 0.0120 s

Then, the model starts to go forward which slows down the blood flow in the venous plexus and even changes its direction downwards, see Figure 57.

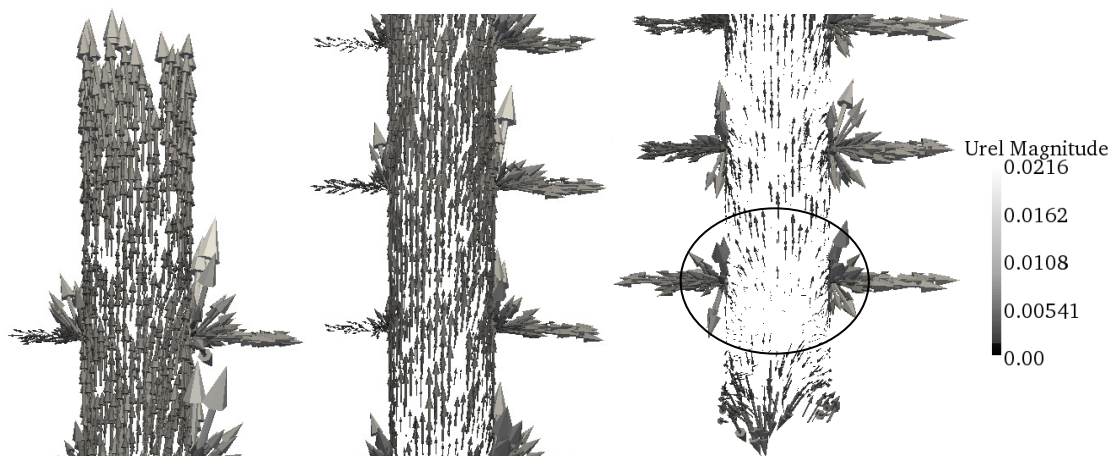


Figure 57 Blood flow through the entire model at 0.0255 s

Afterwards, the point of the position at which the flow changes its direction is moved upwards. At 0.0385 s, it is located in between C5 and C7, see Figure 58.

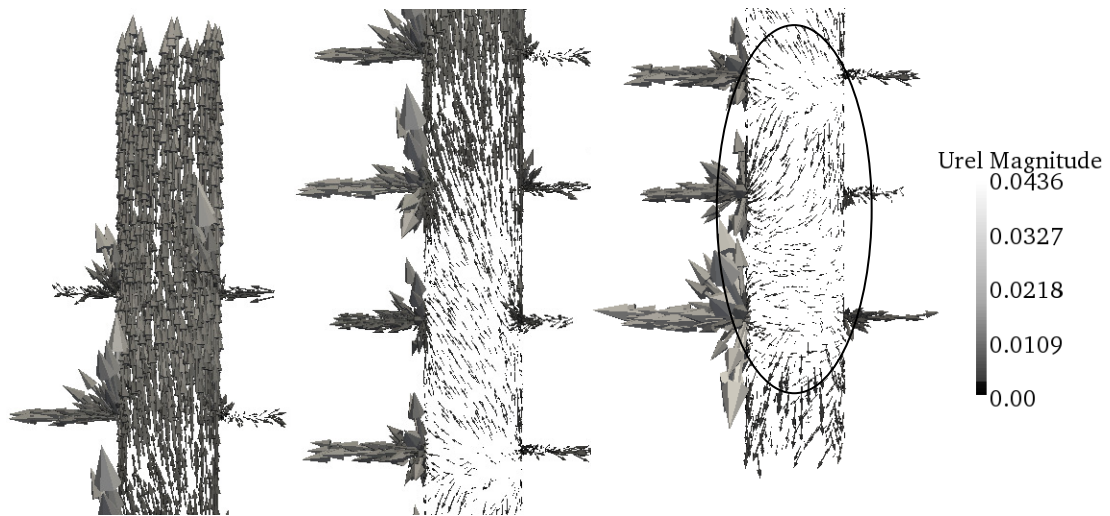


Figure 58 Blood flow through the entire model at 0.0385 s

At 0.0530 s, the point of direction change is between C5 and C6, see Figure 59.

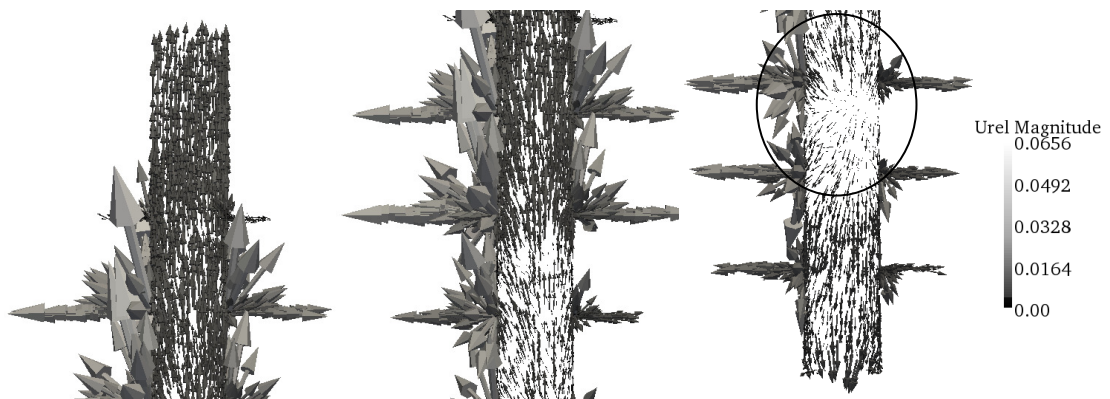


Figure 59 Blood flow through the entire model at 0.0530 s

For 0.0664 s, this point is located between C3 and C6, see Figure 60.

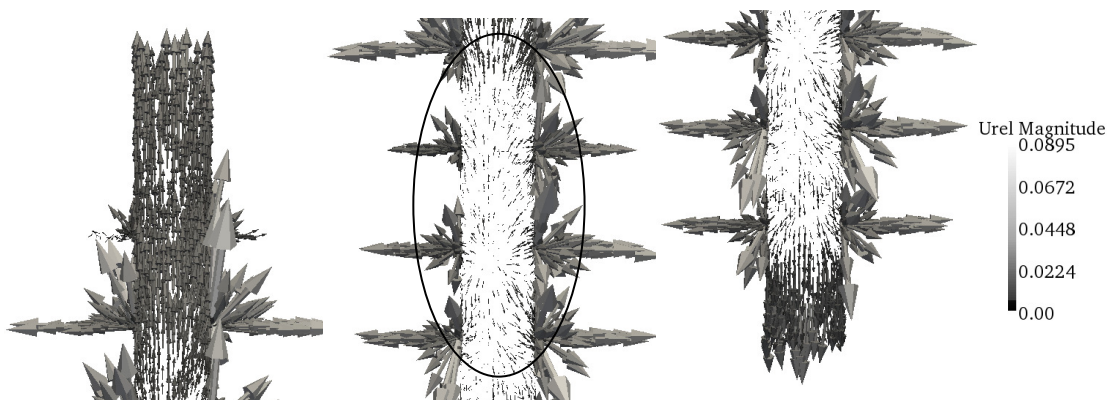


Figure 60 Blood flow through the entire model at 0.0664 s

This point continuously moves upwards, see Figures 61 and 62, until it reaches the uppermost position in the height of C3 vertebra at about 0.1 s, when the maximum extension is occurring, see Figure 63.

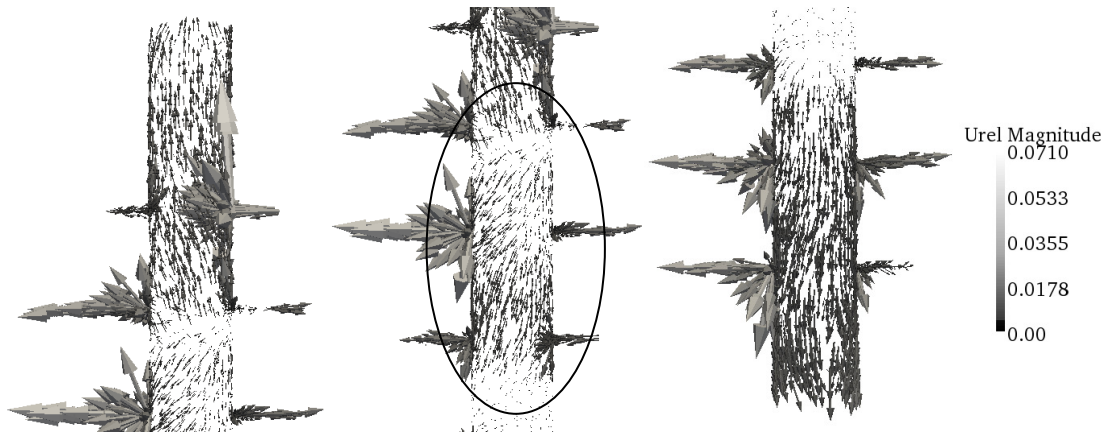


Figure 61 Blood flow through the entire model at 0.0793 s

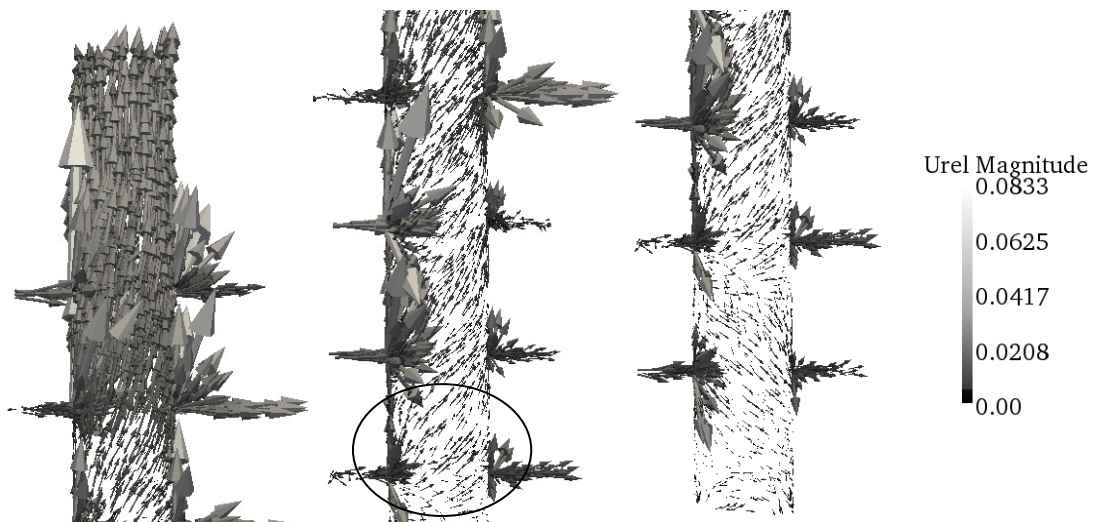


Figure 62 Blood flow through the entire model at 0.0926 s

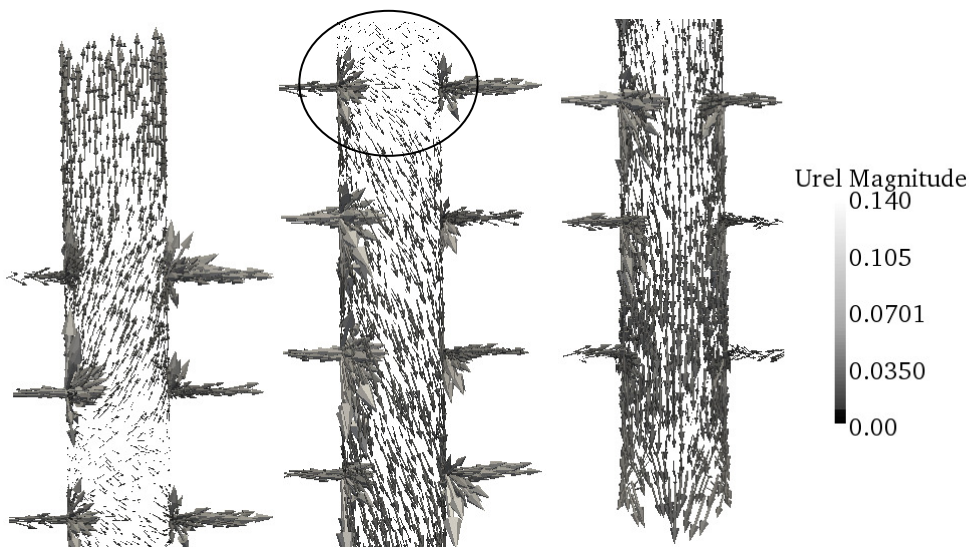


Figure 63 Blood flow through the entire model at 0.1063 s

After the maximum extension of the neck is reached, the point at which flow direction changes goes back downwards, see Figures 64, 65 and 66.

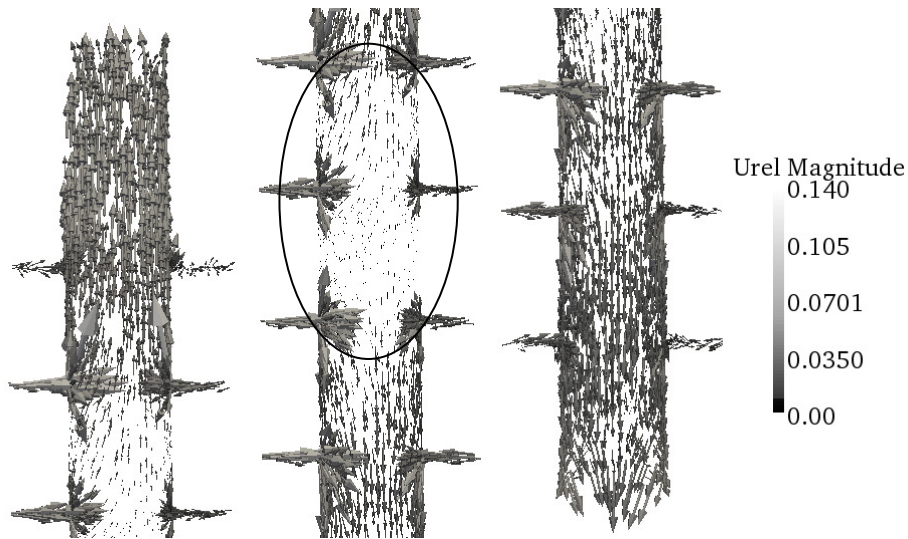


Figure 64 Blood flow through the entire model at 0.1209 s

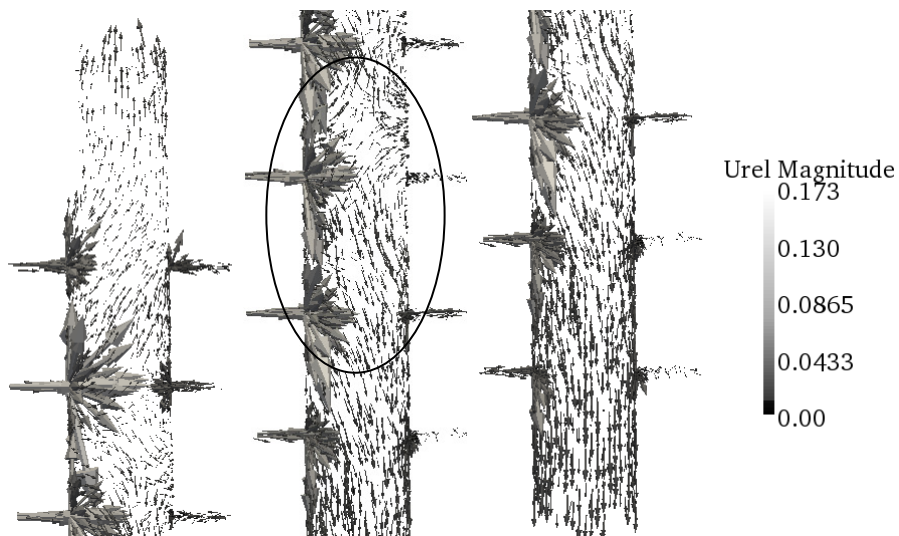


Figure 65 Blood flow through the entire model at 0.1351 s

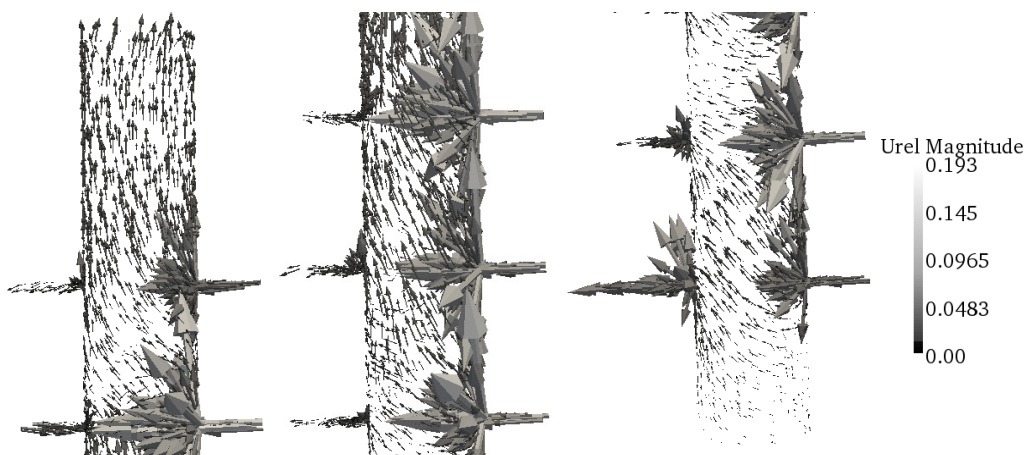


Figure 66 Blood flow through the entire model at 0.1620 s

At 0.1761 s, the flow through the entire model goes upwards, see Figure 67.

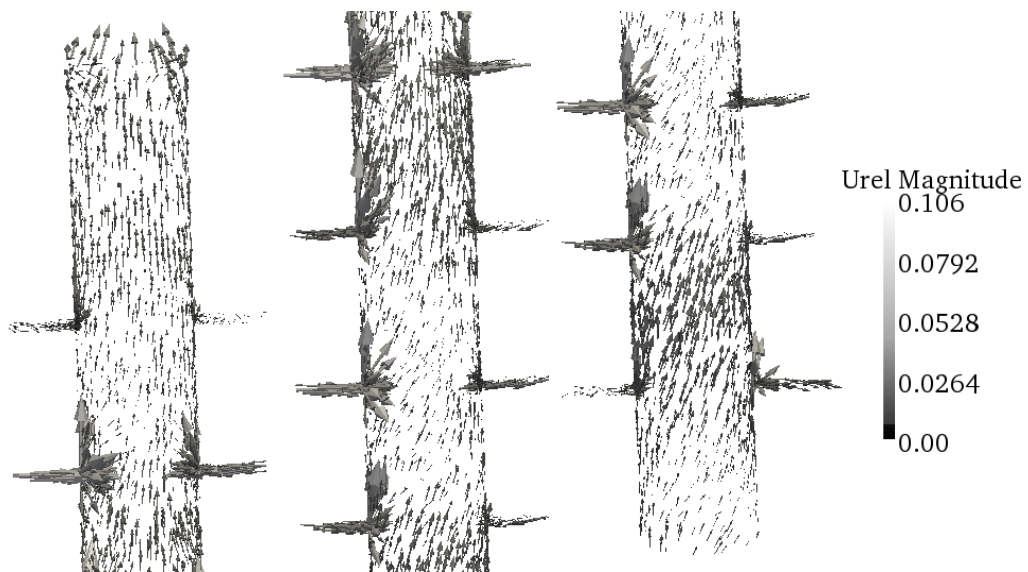


Figure 67 Blood flow through the entire model at 0.1761 s

And after 0.1761 s, the flow will keep this direction while increasing its velocity, see Figures 68 and 69.

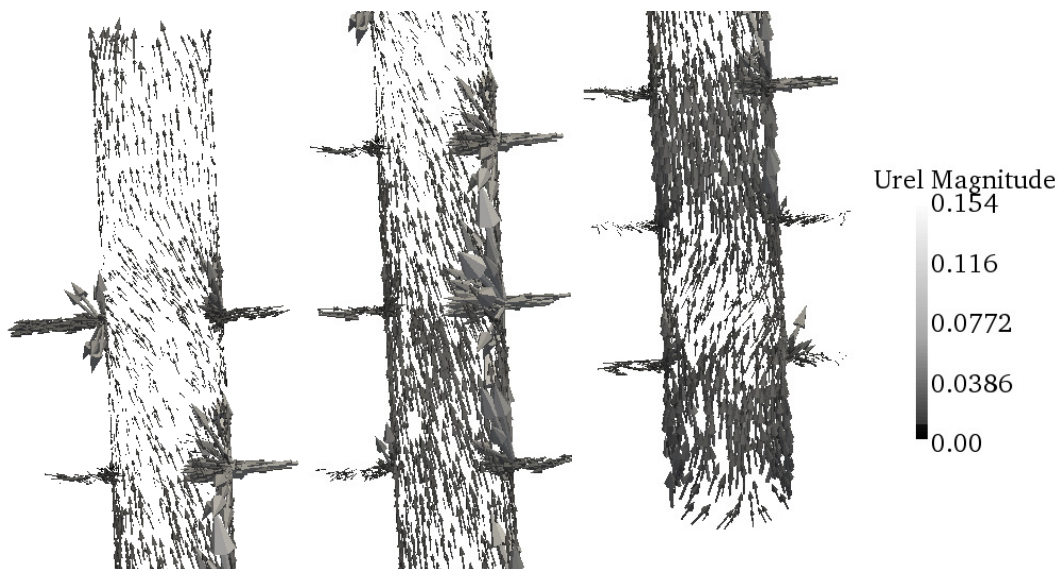


Figure 68 Blood flow through the entire model at 0.1897 s

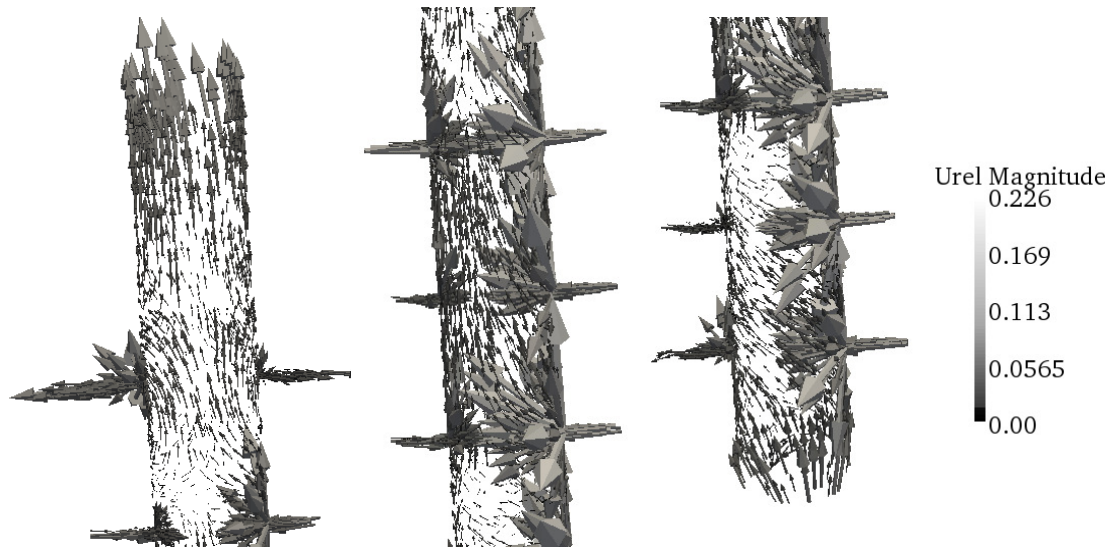


Figure 69 Blood flow through the entire model at 0.2039 s